POROSITY STUDIES AND DETERMINATION OF ELASTIN CONTENT IN CANINE CONNECTIVE TISSUES

POROSITY STUDIES AND DETERMINATION OF ELASTIN CONTENT IN CANINE CONNECTIVE TISSUES

by

Abdul Latiff Ahood

A Thesis

Submitted to the School of Graduate Studies

in Partial Fulfilment of the Requirements

for the Degree

Master of Engineering

McMaster University

Hamilton, Ontario, Canada

1978

ABSTRACT

By means of porosity curves and diffusion equations solved by computer, the microvoid and macrovoid (hence elastin) content of various tissues from the dog are determined. The elastin content is correlated to the stress-strain characteristics of the respective tissues obtained previously (Project I) and the results are supported, to some extent, by histology. The area correction for microvoids are found to be essential for the cases of the abdominal skin and the cornea only. The correction for macrovoids are essential for all the tissues except the Achilles tendon.

ACKNOWLEDGEMENTS

I would like to express my heartfelt gratitude to the following people whose help have been highly instrumental in this work:

Dr. Y.F. Missirlis, my project suprvisor, for his guidance and moral support.

Miss Denise Lamarche for allowing me to use the computer programme developed by her.

The Canadian Commonwealth Scholarship and Fellowship Administration for financing my programme of studies.

To

Douglas Noel

for helping me through the winter of my discontent

TABLE OF CONTENTS

LIST OF TABLES AND FIGURES

INTRODUCTION

1. Importance of Porosity Studies

This work seeks to determine the amount of pores present in the dog's tissues studied in Project I. The native tissues contain natural pores called here micropores whereas the deelastinated tissues contain macropores, apart from the micropores. The amount of macropores in the deelastinated tissues is a measure of the elastin content of the tissue. Knowing the porosity content, the stress-strain characteristics, and histology of a particular tissue will enable us to specify (as close as possible) the physical properties of the tissue. This may be useful in the design of prosthetic devices and possibly also in homograft and heterograft work. The elastin content of a tissue may also be a good indication of its pathological condition (7, 8, 12). These include observations of a rise in incremental Young's modulus with aging (7), possibly caused by an increase in the ratio of collagen to elastin fibres (8); and a general deterioration in the quality of intra-arterial components in vessels affected by arteriosclerosis (8).

2. Prior work

The literature on the determination of elastin content of dog's tissues is rather scarce. Neuman and Logan (9) determined the collagen and elastin content of aorta, liver, kidney, skin etc. of cattle, rat and dog by a chemical method. In this particular paper (9) the only

work done with regards to the dog was the determination of the collagen content of the dog's skin. Lake (6) determined the elastin content of bovine and human aorta by a method similar to the one used in this work.

EXPERIMENTAL PROCEDURES

The equipment used here was a pair of chloride ion electrodes attached to a chart recorder (Sargent Welch, Model SRLG). The electrodes were first calibrated in terms of millivolts (mv) values versus various known concentration (moles/litre) of saline solutions.

A 100 ml portion of deionised water was placed in a beaker and the chloride electrodes were dipped into the deionised water. The water was continuously stirred by a magnetic stirrer.

The tissues to be used were cut into rectangular strips as described in Project I and were equilibrated in saline of known concentration.

The porosity experiment was first performed on the native tissues. The chosen sample was carefully removed from the equilibrating solution by a pair of tweezers holding on to the tissue's edge. The sample was laid on a piece of tissue paper. Another piece of tissue paper was laid on top of the sample. The tissue sample was very gently dabbed to remove the saline solution on its surface. By looking at the tissue through a microscope, it was possible to remove final traces of saline on the surface. Throughout this process it was made sure that the tissue was not squeezed.

The tissue was then transferred to the deionized water surrounding

the chloride electrodes. (The deionized water was stirred continuously by a magnetic stirrer). At the same time a stop watch was started. The diffusion of saline out of the tissue into the deionized water was traced on the chart recorder with the horizontal axis calibrated in seconds and the vertical axis in mV values. Throughout this process the magnetic stirrer was in operation. By means of the chloride electrode calibration curve, a porosity curve of "concentration of chloride ions in moles/100 ml vs "time (seconds)" for the particular tissue sample was obtained.

The experiment was repeated with another sample of approximately the same dimension (from the same tissue) using a fresh sample of deionised water. Altogether five samples of the same tissue (of approximately the same dimension) were treated this way. After this experiment, all the five samples used were deelastinated by the enzymolysis technique described in Project I and reequilibrated in saline of the same concentration as before. Then the whole process was repeated on these deelastinated samples and also on other samples from other tissues. The process was repeated with mucopolysaccharides (MPS)-free tissues as well.

RESULTS

Typical porosity curves for the descending aorta, ascending aorta, Achilles tendon, abdominal skin, cornea and sclera are shown in Figs. 1 to 6 for both the native and deelastinated tissues and also for the MPS-free tissues (Figs. 8-10). Figs. 1-6 also show the theoretical porosity curves for the deelastinated tissues as evaluated by the computer program (see "Theory" and "Computer Program").

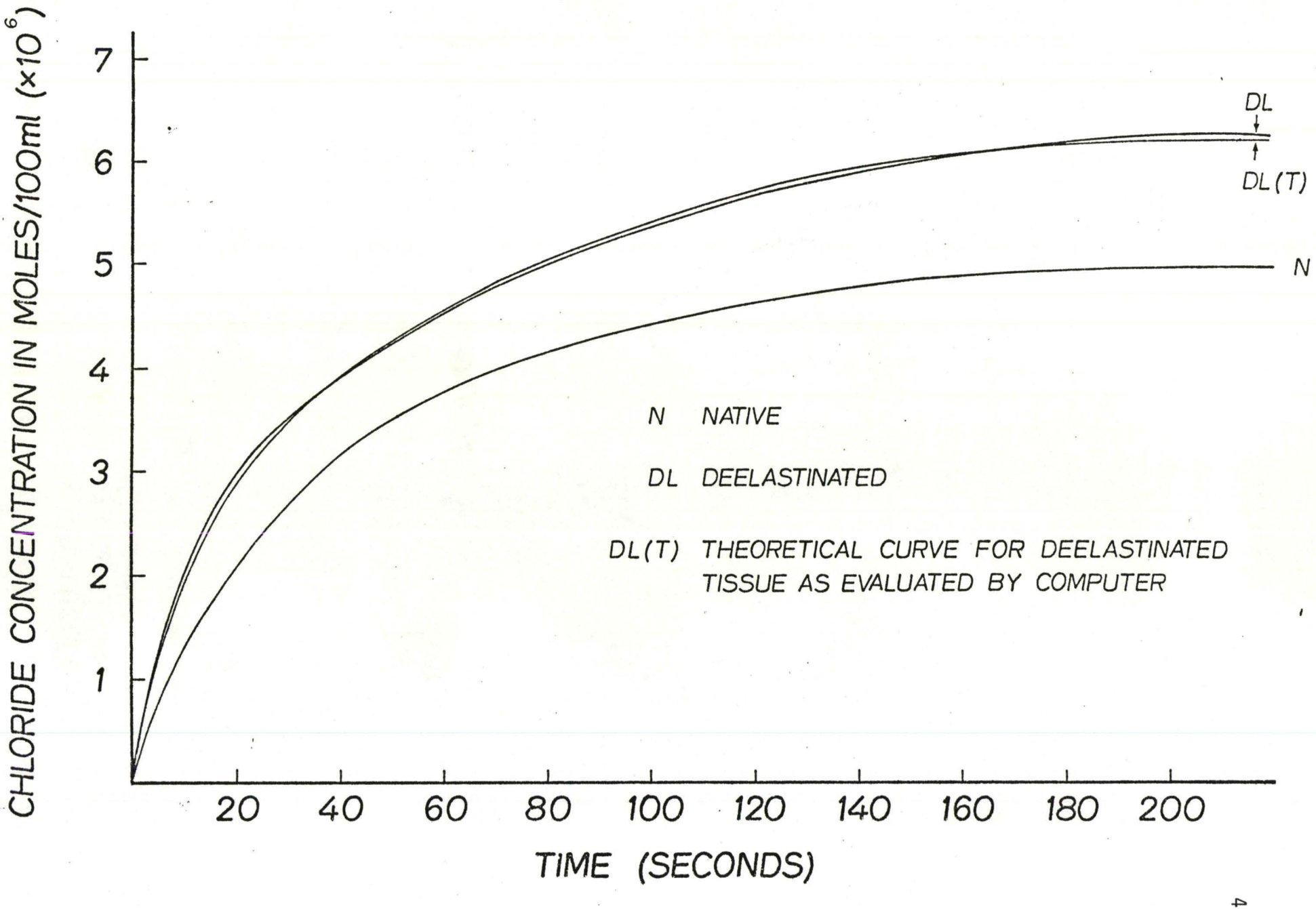

Fig. 1: Typical Porosity Curves for Descending Aorta

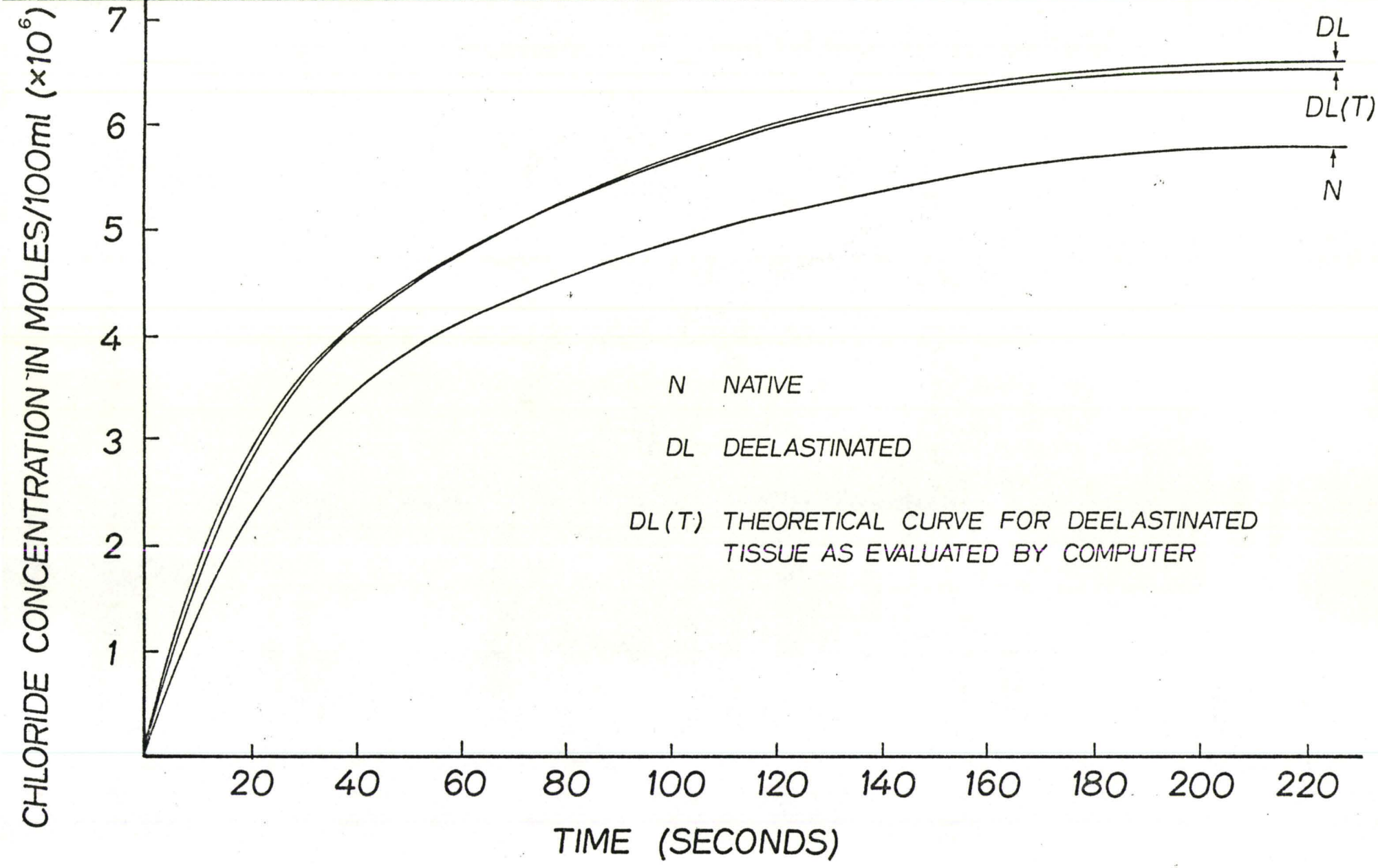

Fig. 2: Typical Porosity Curves for Ascending Aorta

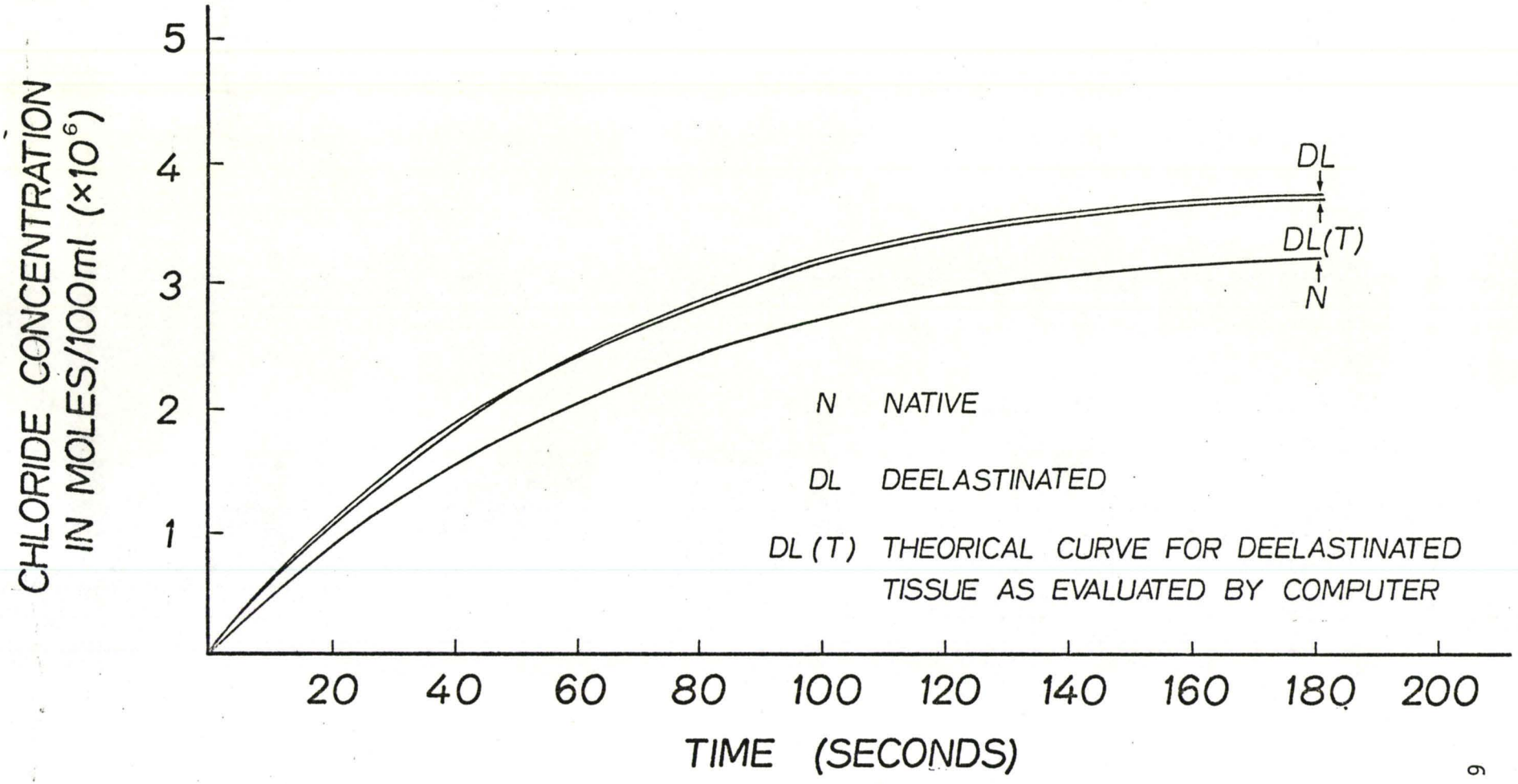

Fig. 3: Typical Porosity Curves for Achilles tendon

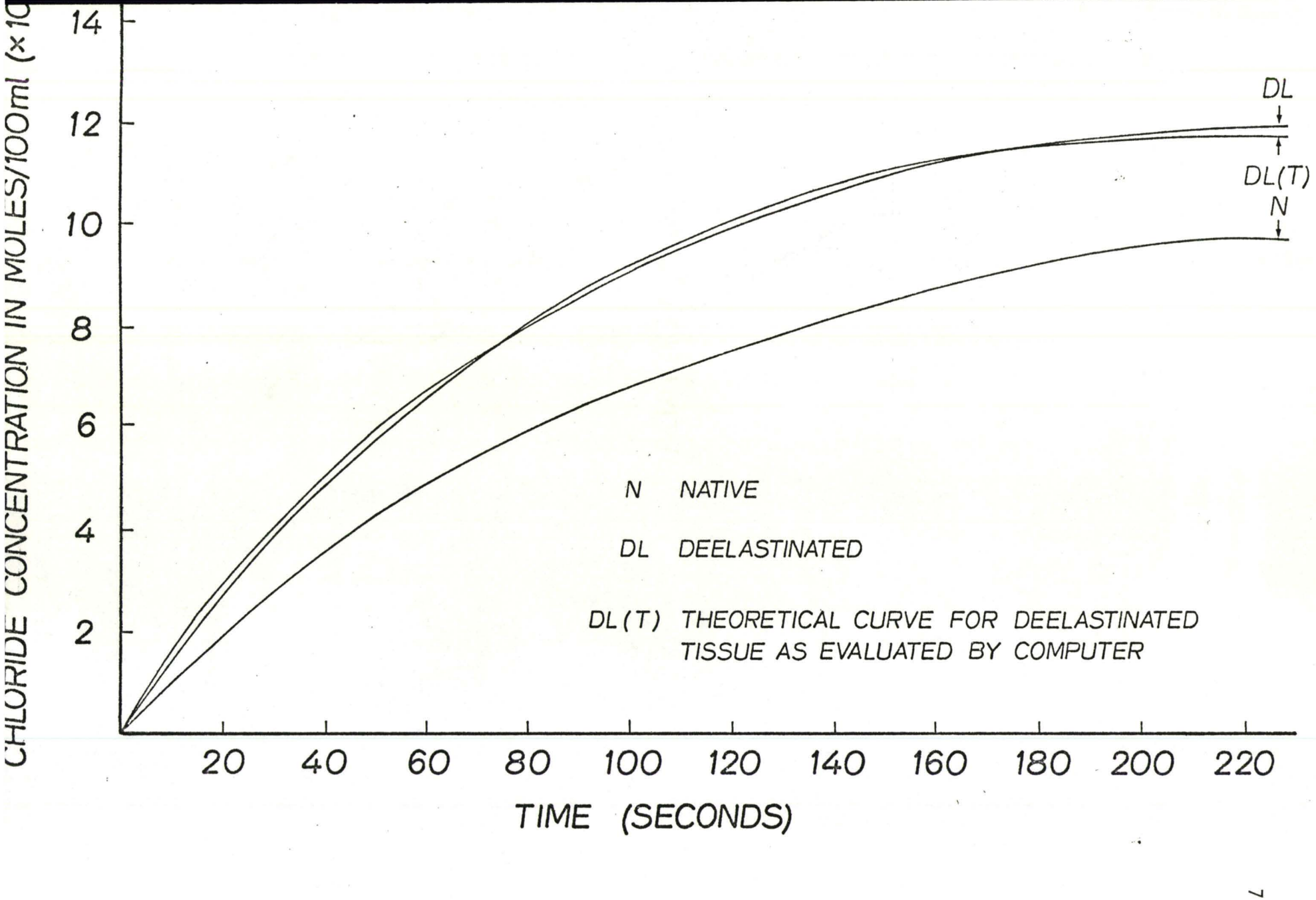

Fig. 4: Typical Porosity Curves for Abdominal Skin

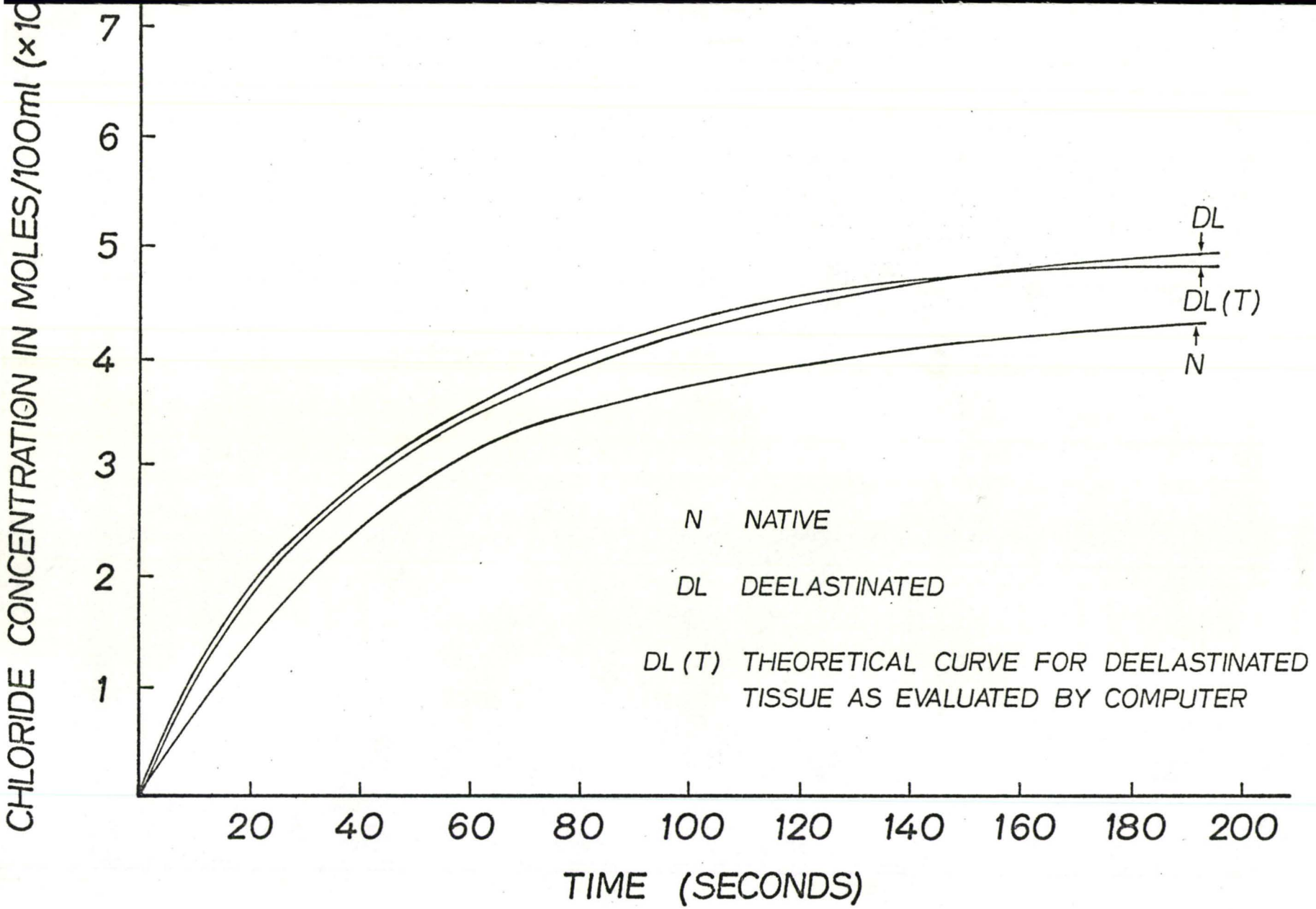

Fig. 5: Typical Porosity Curves for Cornea

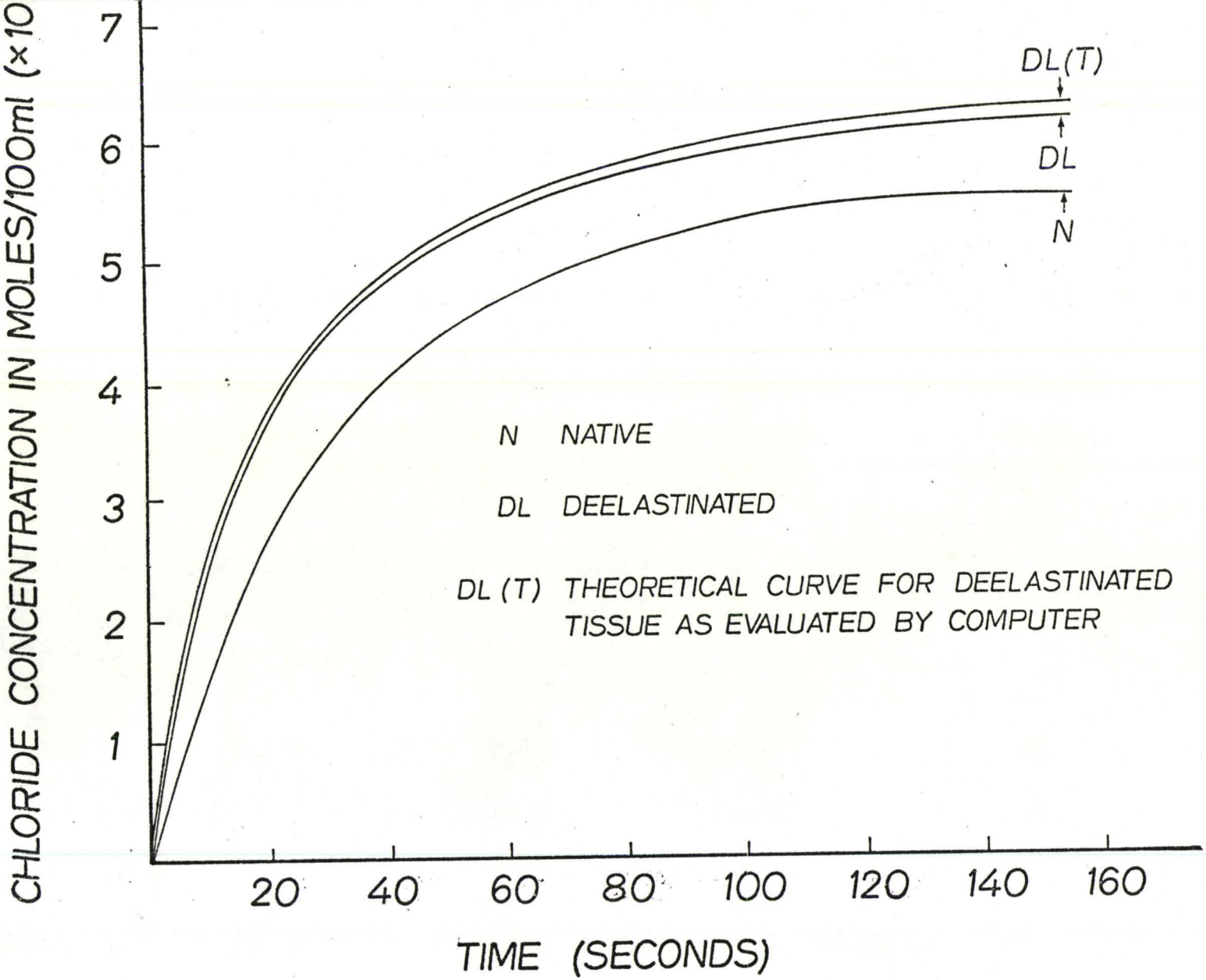

Fig. 6: Typical Porosity Curves for Sclera

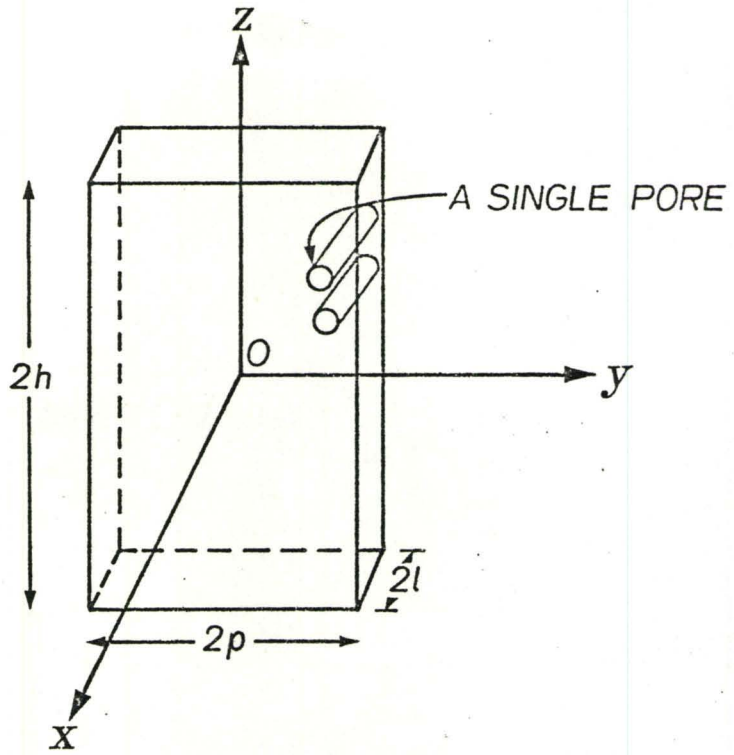

Fig. 7(a): A Tissue Sample with Voids

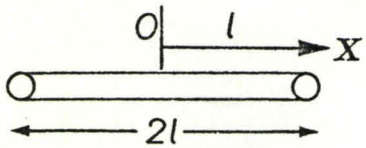

Fig. 7(b): A Single Pore

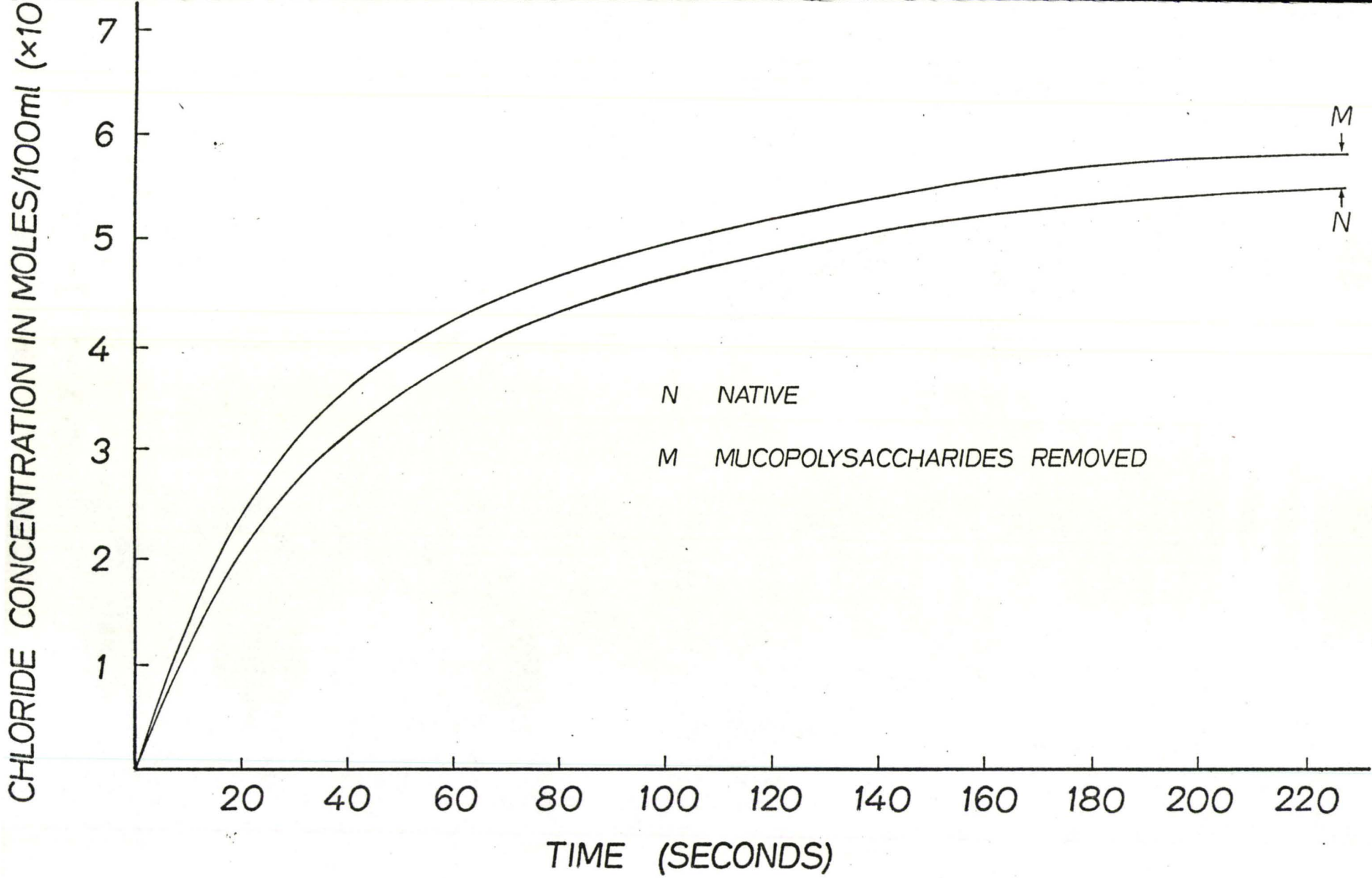

Fig. 8: Typical Porosity Curves for Ascending Aorta

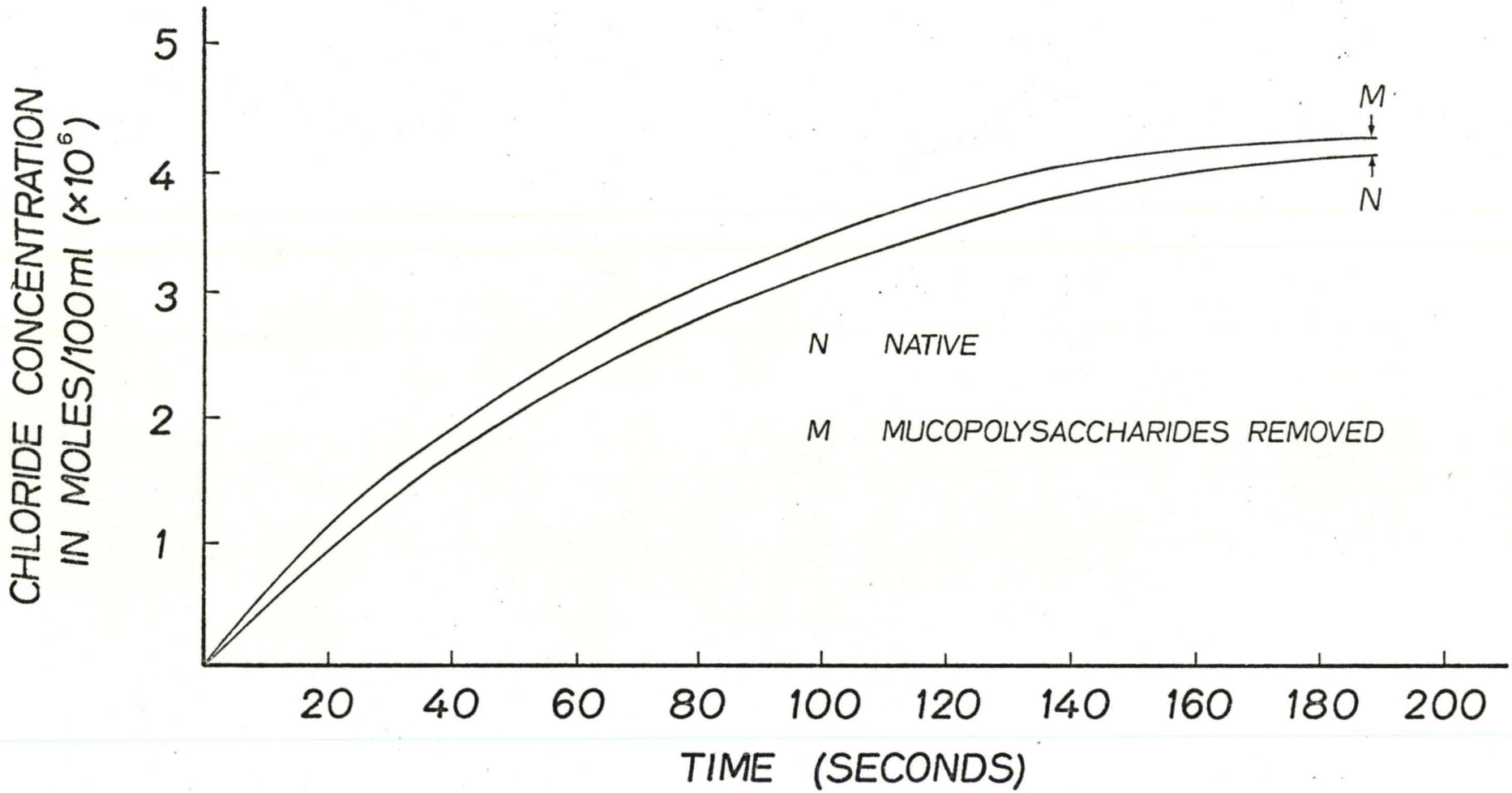

Fig. 9: Typical Porosity Curves for Achilles Tendon

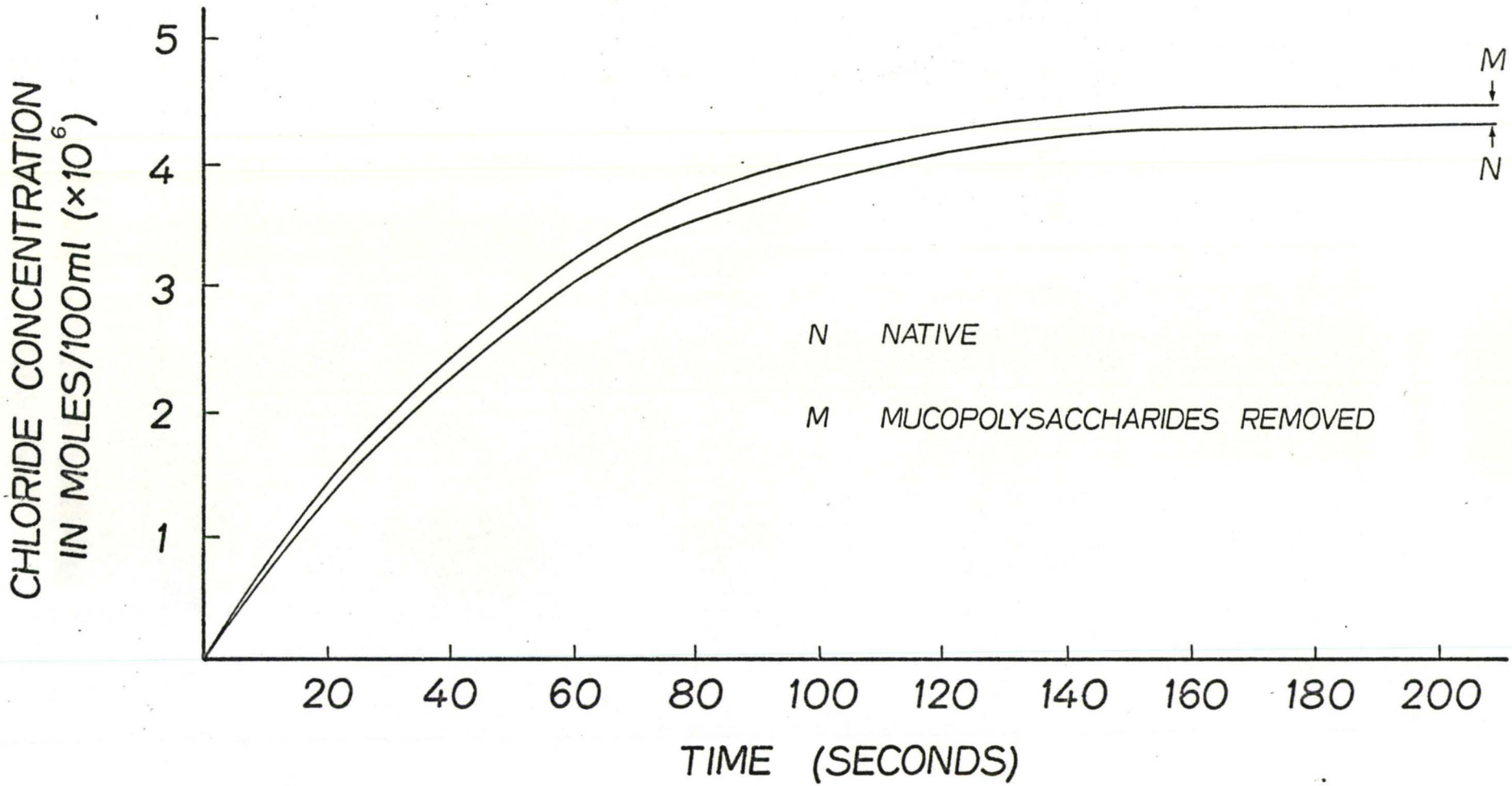

Fig. 10: Typical Porosity Curves for Cornea

THEORY

The following theoretical consideration is taken from Lake (6). Consider a tissue sample soaking in a saline solution of known concentration C_o. At time t = 0, the sample is transferred to a leaching solution (i.e. deionised water in this case) of known volume V_s initially containing no chloride ions. After sufficient time the chloride concentration in the external or leaching solution and in the sample voids equalizes at C_{extf}. Making a mass balance on the chloride yields the void volume V_v,

$$V_v = \frac{C_{extf}}{C_o} V_s \qquad \text{if } V_s >> V_v \tag{1}$$

V_v is the total voids consisting of both macro and microvoids. Since the two voids are considerably different they have to be treated separately.

Consider a tissue sample with pores as shown in Fig. 7. Suppose a Cartesian coordinate system is drawn such that its origin is at the centre of the tissue (Fig. 7). Assume the tissue to contain n pores which are uniformly distributed and that diffusion takes place in the x direction only.

Considering one pore only, for diffusion to occur the governing equation is

$$\frac{\partial C}{\partial t} = D \frac{\partial^2 C}{\partial x^2} \tag{2}$$

where D = diffusion coefficient

C = concentration of chloride ions = C(x,t)

subject to the boundary conditions,

$$C(x,o) = C_o \qquad -\ell < x < \ell \tag{3}$$

$$C = C_{extf} = \text{constant at equilibrium} \tag{4}$$

$$\frac{\partial C(o,t)}{\partial x} = 0, \text{ i.e. flow in the middle} = 0 \tag{5}$$

$$C(x,t) = C(-x,t) \text{ for symmetry} \tag{6}$$

For equation (2) we assume a solution of the form

$$C = C(x,t) = X(x).T(t) \tag{7}$$

i.e. from (2), $\frac{\partial(X.T)}{\partial t} = D\,\frac{\partial^2(XT)}{\partial x^2}$ (8)

$$\text{i.e. } X\frac{dT}{dt} = DT\frac{d^2X}{dx^2} \tag{9}$$

Dividing by XT throughout we have

$$\frac{1}{T}\frac{dT}{dt} = D.\frac{1}{X}\frac{d^2X}{dx^2} = -\mu^2 D \tag{10}$$

where $\mu^2 = -\frac{1}{X}\frac{d^2X}{dx^2}$ (11)

$$\therefore \frac{1}{T}\frac{dT}{dt} = -\mu^2 D$$

$$\text{or } \frac{dT}{T} = -\mu^2 D dt \tag{12}$$

which yields a solution of $T = ae^{-\mu^2 Dt}$ where a is a constant. (13)

From (11) we have $\frac{1}{X}\frac{d^2X}{dx^2} = -\mu^2$ (14)

$$\text{or } \frac{d^2X}{X} = -\mu^2 dx^2 \tag{15}$$

giving a solution of $X = (a'\sin \mu x + b'\cos \mu x)$ (16)

where a', b' are constants.

Now using (7) we have

$$C = (A \sin \mu x + B \cos \mu x)e^{-\mu^2 Dt} \tag{17}$$

where A, B, and μ are constants.

The most general solution is obtained by summing the solution,

$$C(x,t) = \sum_{m=1}^{\infty} (A_m \sin \mu_m x + B_m \cos \mu_m x)e^{-\mu_m^2 Dt} \tag{18}$$

Applying the condition $C(\ell,t) = 0$, we have

$$\sum_{m=1}^{\infty} (A_m \sin \mu_m \ell + B_m \cos \mu_m \ell)e^{-\mu_m^2 Dt} = 0$$

i.e. $A_m \sin \mu_m \ell + B_m \cos \mu_m \ell = 0$

Applying condition (5) we obtain

$$\frac{\partial C(o,t)}{\partial x} = 0 = \sum_{m=1}^{\infty} \mu_m (A_m \cos o - B_m \sin o)e^{-\mu_m^2 Dt}$$

from which

$$A_m = 0$$

$$\therefore C(x,t) = \sum_{1}^{\infty} B_m \cos \mu_m x e^{-\mu_m^2 Dt}$$

Again applying $C(\ell,t) = 0$ we obtain

$$B_m \cos \mu_m \ell = 0$$

or $$\mu_m \ell = \frac{m\pi}{2}$$

hence $\mu_m = \frac{m\pi}{2\ell}$ (19)

$$C(x,t) = \sum_{1}^{\infty} B_m \cos \frac{m\pi x}{2\ell} \, e^{-(m\pi/2\ell)^2 Dt} \tag{20}$$

Applying condition (3) we have

$$C(x,o) = C_o = \sum_{1}^{\infty} B_m \cos \frac{m\pi x}{2\ell} \tag{21}$$

Multiplying both sides by $\cos \frac{p\pi x}{2\ell}$ results in

$$C_o \cos \frac{p\pi x}{2\ell} = \sum_{1}^{\infty} B_m \cos \frac{m\pi x}{2\ell} \cos \frac{p\pi x}{2\ell}$$

Integrating from centre of tissue to ℓ

$$C_o \int_o^{\ell} \cos \frac{p\pi x}{2\ell} \, dx = \sum_{1}^{\infty} B_m \int_o^{\ell} \cos \frac{m\pi x}{2\ell} \cos \frac{p\pi x}{2\ell} \, dx \tag{22}$$

If $p \neq m$, $\int_o^{\ell} \cos \frac{m\pi x}{2\ell} \cos \frac{p\pi x}{2\ell} \, dx = 0$

If $p = m$, we obtain

$$\sum_{1}^{\infty} C_o \int_o^{\ell} \cos \frac{m\pi x}{2\ell} \, dx = \sum_{1}^{\infty} B_m \int_o^{\ell} \cos^2 \frac{m\pi x}{2\ell} \, dx$$

Carrying out the integration yields

$$\sum_{1}^{\infty} \frac{2\ell}{m\pi} C_o \sin \frac{m\pi x}{2\ell} \Big]_o^{\ell} = \sum_{1}^{\infty} B_m \frac{2\ell}{m\pi} \left(\frac{m\pi x}{4\ell} + \frac{1}{4} \sin \frac{m\pi x}{\ell} \right) \Big]_o^{\ell}$$

Substituting limits gives

$$\sum_{1}^{\infty} \frac{2\ell}{m\pi} C_o \left(\sin \frac{m\pi}{2} - \sin o\right) = \sum_{1}^{\infty} B_m \frac{2\ell}{m\pi} \left(\frac{m\pi}{4} + \frac{1}{4} \sin m\pi - 0 - \frac{1}{4} \sin o\right)$$

Simplifying

$$\frac{2\ell}{m\pi} C_o \sin \frac{m\pi}{2} = B_m \frac{2\ell}{m\pi} \cdot \frac{m\pi}{4}$$

i.e. $B_m = \frac{4}{m\pi} C_o \sin \frac{m\pi}{2} = 0$ for even values of m

$$= \frac{4C_o}{\pi m} \quad \text{for odd values of m}$$

$$\therefore B_m = \frac{4C_o}{m\pi} \quad \text{for odd m} \tag{23}$$

i.e. $$C(x,t) = \sum_{m} \frac{4C_o}{m\pi} \cos \frac{m\pi x}{2\ell} e^{-(m\pi/2\ell)^2 Dt} \tag{24}$$

Put $m = 2m' + 1$ where $m' = 0, 1, 2, 3, \ldots$ (25)

$$\therefore C(x,t) = \sum_{m'} \frac{4C_o}{(2m'+1)} \cos \frac{(2m'+1)}{2\ell} \pi x . e^{-(2m'+1)^2 \left(\frac{\pi}{2\ell}\right)^2 Dt} \tag{26}$$

or $$C(x,t) = \sum_{o}^{\infty} \frac{4C_o}{(2m'+1)} \cos \frac{(2m'+1)}{2\ell} \pi x . e^{-(2m'+1)^2 \left(\frac{\pi}{2\ell}\right)^2 Dt} \tag{27}$$

Taking only the first term of the summation (i.e. $m' = 0$) we have

$$C(x,t) = 4C_o \cos \frac{\pi x}{2\ell} e^{-(\pi/2\ell)^2 Dt} \tag{28}$$

The relation between C_{ext} (external concentration of chloride ions in leaching solution) and C(x,t) is given by:

$$V_s \left(\frac{dC_{ext}}{dt}\right) = -D \pi r^2 n \left(\frac{\partial C}{\partial x}\right)_{x=\ell} \tag{29}$$

where r = radius of pore

n = number of pores

$$\text{i.e.} \quad \frac{dC_{ext}}{dt} = \frac{-D\pi r^2 n}{V_s}\left\{-4C_o \cdot \frac{\pi}{2\ell} \sin\frac{\pi\ell}{2\ell} e^{-(\pi/2\ell)^2 Dt}\right\} \tag{30}$$

by differentiating (28) at $x = \ell$.

Rearranging: $\frac{dC_{ext}}{dt} = \frac{2\pi^2 r^2 Dn}{V_s \ell} C_o e^{-(\pi/2\ell)^2 Dt}$

Integrating from 0 to t we have

$$\int_o^t dC_{ext} = \frac{2\pi^2 r^2 DnC_o}{V_s \ell} \int_o^t e^{-(\pi/2\ell)^2 Dt} dt$$

$$\text{i.e.} \quad C_{ext}(t) = \frac{2\pi^2 r^2 DnC_o}{V_s \ell}\left\{-\left(\frac{2\ell}{\pi}\right)^2 \cdot \frac{1}{D} e^{-(\pi/2\ell)^2 Dt}\right\}_o^t$$

Substituting limits gives

$$C_{ext}(t) = \frac{2\pi^2 r^2 DnC_o}{V_s \ell} \frac{4\ell^2}{\pi^2} \frac{1}{D}\left\{1 - e^{-(\pi/2\ell)^2 Dt}\right\}$$

$$\text{i.e.} \quad C_{ext}(t) = \frac{8r^2 \ell n C_o}{V_s}\left\{1 - e^{-(\pi/2\ell)^2 Dt}\right\} \tag{31}$$

At equilibrium $C_{ext} = C_{extf} = \frac{V_v C_o}{V_s}$

Also $C_{ext}(\infty) = \frac{8r^2 \ell n C_o}{V_s}\left\{1 - e^{-\infty}\right\} = \frac{8r^2 \ell n C_o}{V_s}$ which must equal to C_{extf}

$$\therefore \frac{C_{ext}(t)}{C_{extf}} = \left\{1 - e^{-(\pi/2\ell)^2 Dt}\right\} \tag{32}$$

Equation (32) shows that for $t \to \infty$,

$$\frac{C_{ext}(\infty)}{C_{extf}} = 1 - e^{-\infty} = 1$$

From Taylor's series we have $e^x = 1 + x + \frac{x^2}{2!} + \ldots$

and for small x, $e^x = 1 + x$ ignoring powers higher than the first.

Similarly for small t

$$\frac{C_{ext}(t)}{C_{extf}} = 1 - \{1 - \left(\frac{\pi}{2\ell}\right)^2 Dt\} = \left(\frac{\pi}{2\ell}\right)^2 Dt$$

$$\therefore \frac{C_{ext}(t)}{C_{extf}} = \left(\frac{\pi}{2\ell}\right)^2 Dt \quad \text{for small } t \tag{33}$$

Since $C_{extf} = \frac{V_v C_o}{V_s}$, $V_v = \frac{V_s C_{extf}}{C_o}$ (34)

Substituting (33) we have $V_v = \frac{V_s}{C_o} \frac{(2\ell)^2}{\pi^2 D} \frac{C_{ext}(t)}{t}$ for small t

Otherwise

$$C_{ext}(t) = \frac{C_o V_v}{V_s} \{1 - e^{-(\pi/2\ell)^2 Dt}\} \quad \text{from (32) and (34),}$$

from which

$$V_v = \frac{C_{ext}(t)}{C_o} \left[\frac{V_s}{1 - e^{-(\pi/2\ell)^2 Dt}}\right] \tag{35}$$

The deelastinated tissues contain both microvoids and macrovoids

Let volume of microvoids = $V_1 = \pi r_1^2 (2\ell) n_1$

and volume of macrovoids = $V_2 = \pi r_2^2 (2\ell) n_2$ = volume of elastin.

Let D_1 be the diffusion coefficient due to microvoids, and

D_2 be due to macrovoids, where

r_1 = radius of microvoid pore

r_2 = radius of macrovoid pore

2ℓ = length of pore (or thickness of tissue, see Fig. 7)

n_1 = number of microvoid pores

n_2 = number of macrovoid pores

As before the diffusion equations are:

$$C_1(x,t) = 4C_o \cos \frac{\pi x}{2\ell} e^{-(\pi/2\ell)^2 D_1 t} \text{ for micropores}$$

and $$C_2(x,t) = 4C_o \cos \frac{\pi x}{2\ell} e^{-(\pi/2\ell)^2 D_2 t} \text{ for macropores}$$

Using (29) we have, for both kinds of voids

$$V_s \left[\frac{dC_{ext}}{dt}\right] = -D_1 \pi r_1^2 n_1 \left[\frac{\partial C_1}{\partial x}\right]_{x=\ell} - D_2 \pi r_2^2 n_2 \left[\frac{\partial C_2}{\partial x}\right]_{x=\ell}$$

$$\therefore V_s \int_o^t \frac{dC_{ext}}{dt} = -D_1 \pi r_1^2 n_1 \left[-4C_o \frac{\pi}{2\ell} \sin \frac{\pi \ell}{2\ell} e^{-(\pi/2\ell)^2 D_1 t}\right] - D_2 \pi r_2^2 n_2$$

$$\left[-4C_o \frac{\pi}{2\ell} \sin \frac{\pi \ell}{2\ell} e^{-(\pi/2\ell)^2 D_2 t}\right]$$

Integrating and substituting limits, we obtain

$$C_{ext}(t) = \frac{4C_o}{V_s} \frac{\pi^2 r_1^2 n_1 D_1}{2\ell} \left[-\left(\frac{2\ell}{\pi}\right)^2 \frac{1}{D_1} e^{-(\pi/2\ell)^2 D_1 t}\right]_o^t + \frac{4C_o \pi^2 r_2^2 n_2 D_2}{V_s \; 2\ell}$$

$$\left[-\left(\frac{2\ell}{\pi}\right)^2 \frac{1}{D_2} e^{-(\pi/2\ell)^2 D_2 t}\right]_o^t$$

$$= \frac{4C_o r_1^2 n_1(2\ell)}{V_s}\left[1 - e^{-(\pi/2\ell)^2 D_1 t}\right] + \frac{4C_o r_2^2 n_2(2\ell)}{V_s}$$

$$\left[1 - e^{-(\pi/2\ell)^2 D_2 t}\right]$$

i.e. $$C_{ext}(t) = \frac{4C_o}{V_s}\left[r_1^2 n_1(2\ell)\{1 - e^{-(\pi/2\ell)^2 D_1 t}\} + r_2^2 n_2(2\ell)\{1 - e^{-(\pi/2\ell)^2 D_2 t}\}\right]$$

We know that $\lim_{t\to\infty} \frac{C_{ext}(t)}{C_{extf}} = 1$ and $\lim_{t\to o} \frac{C_{ext}(t)}{C_{extf}} = 0$

Also $C_{extf} = \frac{V_v C_o}{V_s}$ and $V_v = V_1 + V_2 = \pi r_1^2 n_1(2\ell) + \pi r_2^2 n_2(2\ell)$

$$C_{ext}(\infty) = \frac{4C_o}{V_s}\left[r_1^2 n_1(2\ell) + r_2^2 n_2(2\ell)\right]$$

$$\therefore \frac{C_{ext}(\infty)}{C_{extf}} = \frac{4C_o}{V_s}\left[r_1^2 n_1(2\ell) + r_2^2 n_2(2\ell)\right].\frac{V_s}{C_o \pi[r_1^2 n_1(2\ell) + r_2^2 n_2(2\ell)}$$

$$= 4/\pi$$

Since $\lim_{t\to\infty} \frac{C_{ext}(t)}{C_{extf}} = 1$, we must multiply $C_{ext}(t)$ by $\frac{\pi}{4}$

$$C_{ext}(t) = \frac{C_o}{V_s}\left[\pi r_1^2 n_1(2\ell)\{1 - e^{-(\pi/2\ell)^2 D_1 t}\} + \pi r_2^2 n_2(2\ell)\right.$$

$$\left.\{1 - e^{-(\pi/2\ell)^2 D_2 t}\}\right] \qquad (36)$$

i.e. $$C_{ext}(t) = \frac{C_o}{V_s}\left[V_1\{1 - e^{-(\pi/2\ell)^2 D_1 t}\} + V_2\{1 - e^{-(\pi/2\ell)^2 D_2 t}\}\right] \qquad (37)$$

where V_1 = volume of microvoids, and V_2 = volume of macrovoids. Equation (37) can be rewritten as

$$C_{ext}(t) = \frac{C_o V_1}{V_s}\left[1 - e^{-(\pi/2\ell)^2 D_1 t}\right] + \frac{C_o V_2}{V_s}\left[1 - e^{-(\pi/2\ell)^2 D_2 t}\right] \quad (38)$$

Computer Programme

Equation (38) is solved by computer to find V_1 and V_2. The computer program together with a sample output is included in the Appendix of this report. The input to the program are values of time (seconds) and the corresponding chloride ion concentration as obtained from the porosity curves of each deelastinated tissue. The initial values of D_1 and D_2 are also given as input, the values being chosen on a trial and error basis. By a series of iterative procedures, the program computes the "best fit" values to the porosity curves and also values of D_1 and D_2. Hence the output gives a series of values for V_1, V_2, best fit values of chloride ion concentration corresponding to given times, and values for D_1 and D_2 (see Appendix for details). The best fit values of chloride ion concentration vs. time for the deelastinated tissues are shown together with the experimental deelastinated tissues porosity curves in Figs. 1-6.

Computer Results

The computer program computes the microvoid (V_1) and macrovoid (V_2) volumes. The sum of V_1 and V_2 gives the total voids in the tissue after deelastination. The macrovoid (i.e. elastin) content in a tissue can also be estimated from the histological micrographs. The elastin

parts are cut out from the native tissue micrographs and weighed. This weight is then expressed as a percentage weight of the whole micrograph. These two results are compared in Table 1.

Table 1 shows the percent microvoids and macrovoids in the various tissues together with the estimate of percentage elastin (which is a measure of the percentage macrovoids) from histological micrographs from Project I. This is done by making a photocopy of the desired micrograph of the native tissue. The elastin parts are cut out and weighed. This weight is then expressed as a percentage weight of the whole micrograph photocopy. The "Histology" column of Table 1 shows two figures each for the descending aorta, ascending aorta, and abdominal skin which indicates the number of histological estimates made for the above mentioned tissues.

Fig. 11 shows the photocopies of the micrographs used in the histological estimate of elastin in Table 1. For each of the descending aorta, ascending aorta and abdominal skin, the whole micrograph photocopy is shown together with the elastin parts which have been cut out from the micrograph photocopy of the native tissue.

For the cases of the Achilles tendon, cornea and sclera the histological micrographs of the native tissues did not show any trace of elastin. When these tissues were decollagenated their histology micrographs showed a delicate, though somewhat discontinuous, network of elastin fibres as shown in Figs. 12, 13, and 14 (see also "Discussion").

Now that we know the microvoid and macrovoid content of the various tissues the stress-strain curves can be corrected. The corrected values of the high strain moduli of the various tissues are shown in Table 2. This is done by taking the mean values of the high strain moduli (from

Fig. 11(a): Photocopy of Histological Micrograph of Native Descending Aorta (Circumferential Sample)

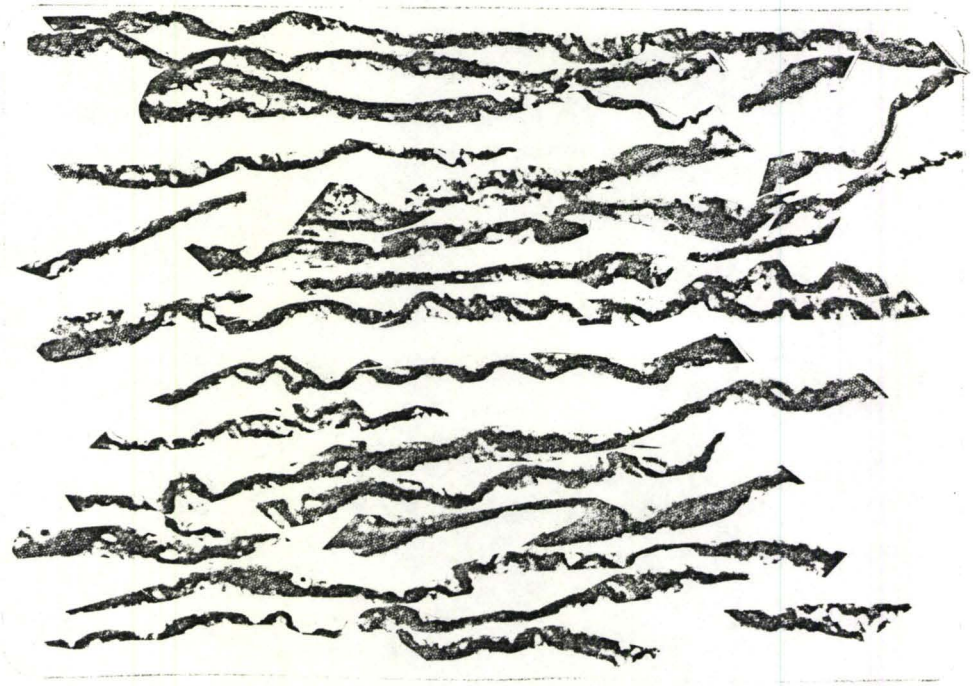

Fig. 11(b): Elastin Parts Cut Out from Fig. 11(a) giving an Elastin Content of 20%

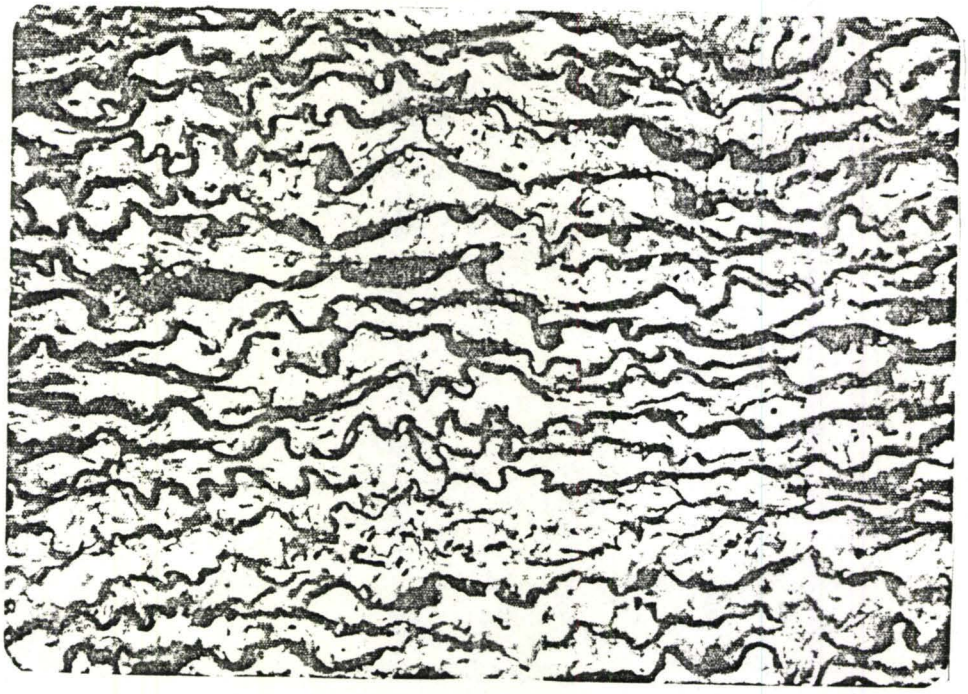

Fig. 11(c): Photocopy of Histological Micrograph of Native Descending Aorta (Longitudinal Sample)

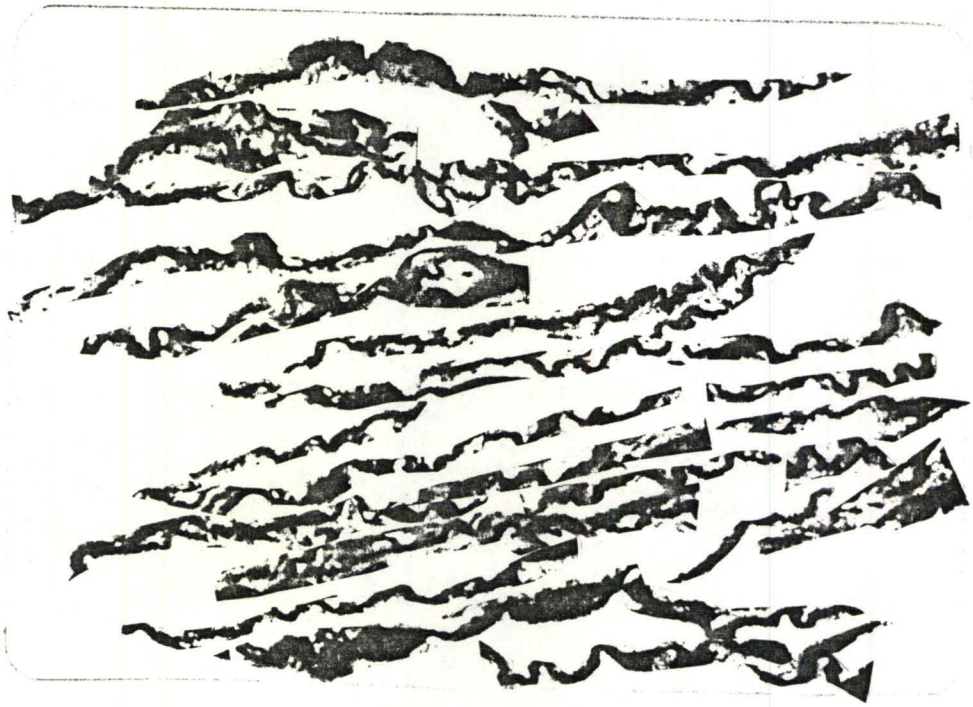

Fig. 11(d): Elastin Parts Cut Out From Fig. 11(c) giving an Elastin Content of 23%

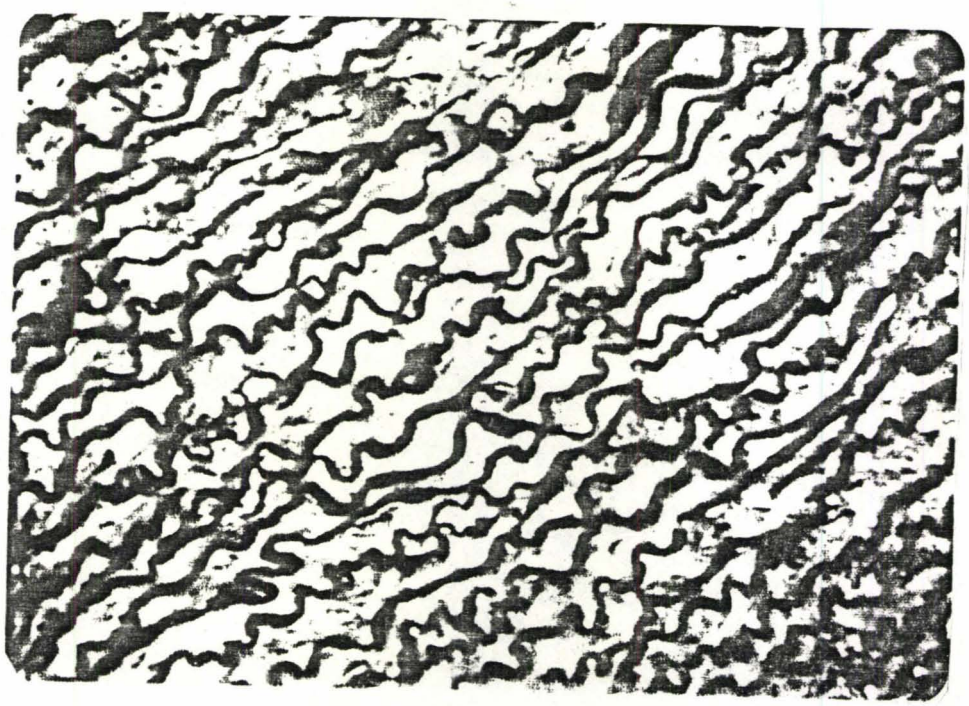

Fig. 11(e): Photocopy of Histological Micrograph of Native Ascending Aorta (Circumferential Sample)

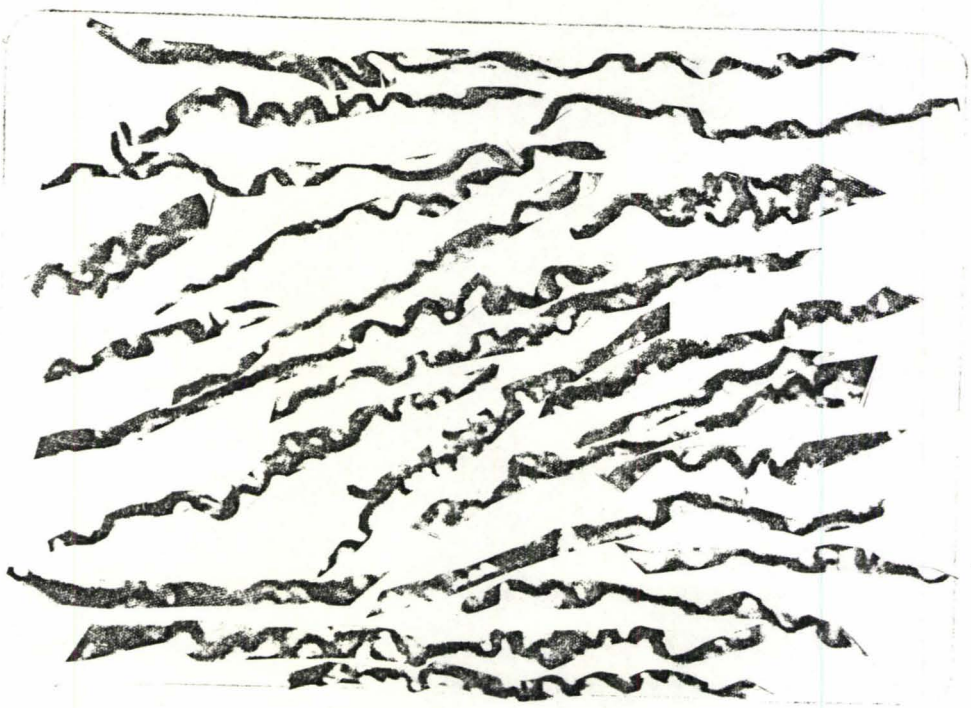

Fig. 11(f): Elastin Parts Cut Out From Fig. 11(e) Giving an Elastin Content of 16%

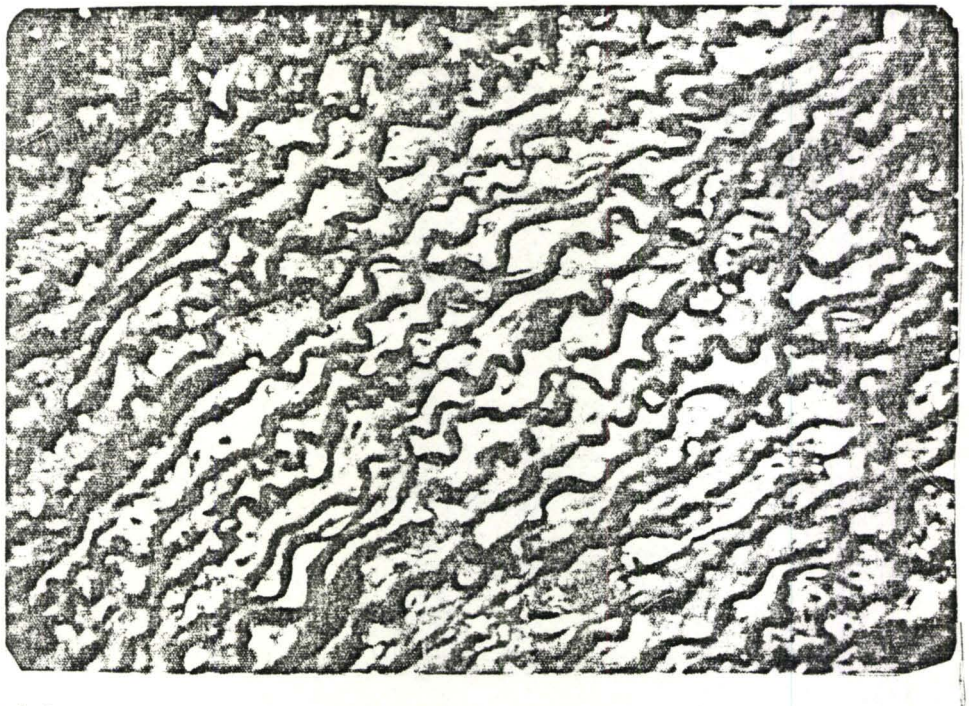

Fig. 11(g): Photocopy of Histological Micrograph of Native Ascending Aorta (Longitudinal Sample)

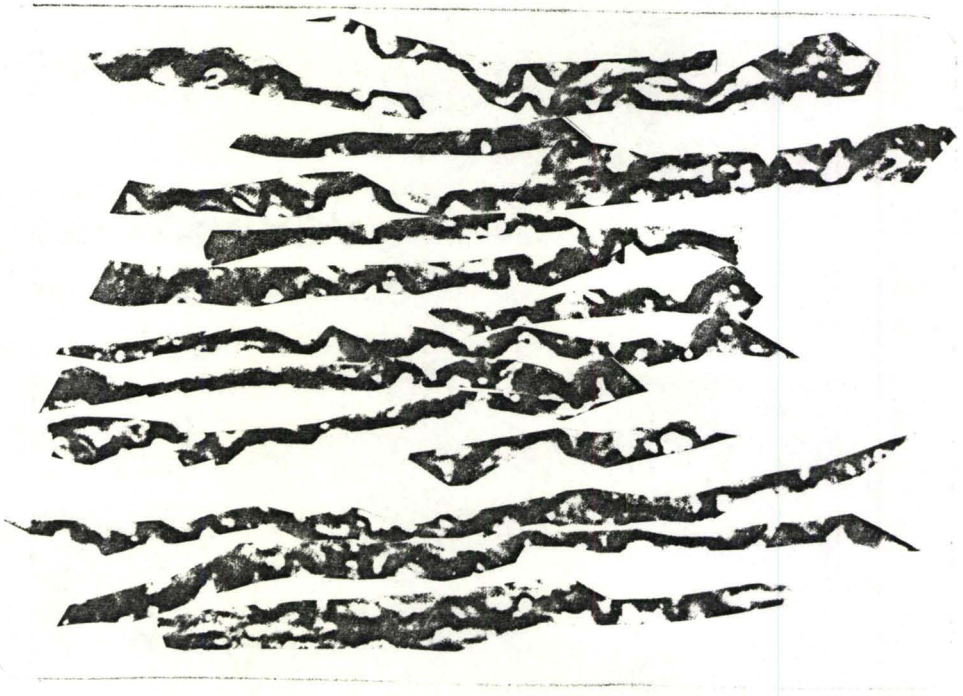

Fig. 11(h): Elastin Parts Cut Out From Fig. 11(g) Giving an Elastin Content of 14%

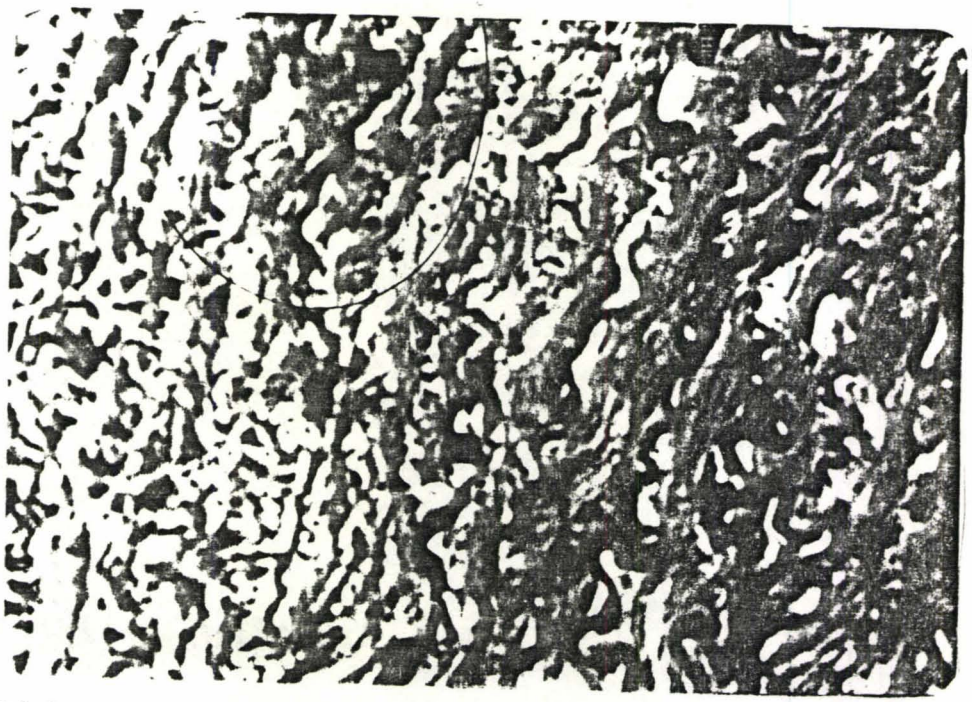

Fig. 11(i): Photocopy of Histological Micrograph of Native Abdominal Skin (Longitudinal Sample)

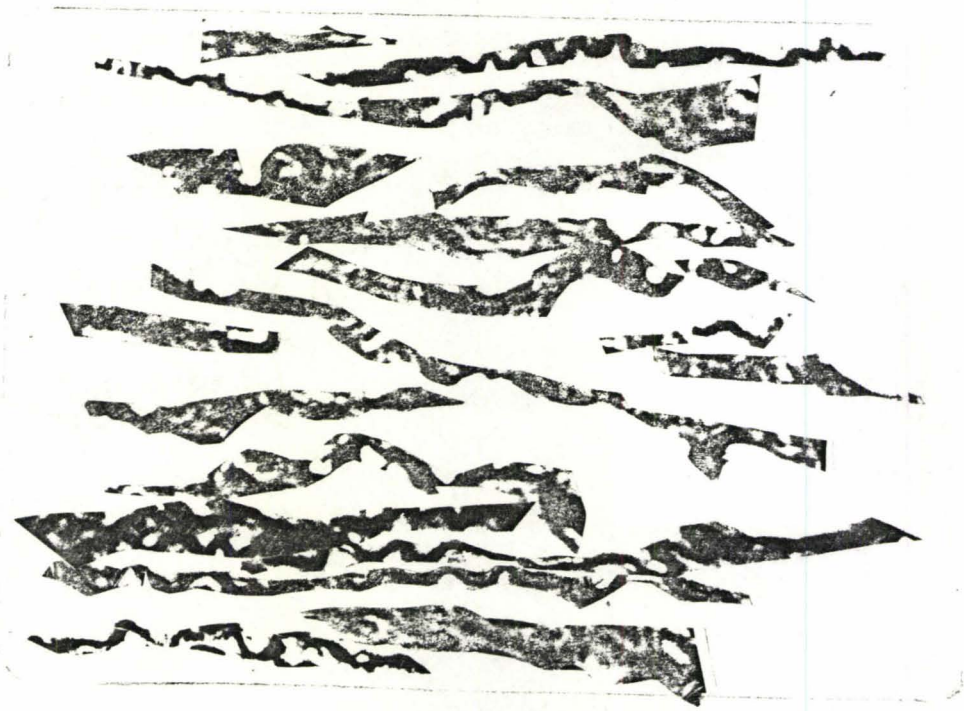

Fig. 11(j): Elastin Parts cut Out From Fig. 11(i) Giving an Elastin Content of 19%

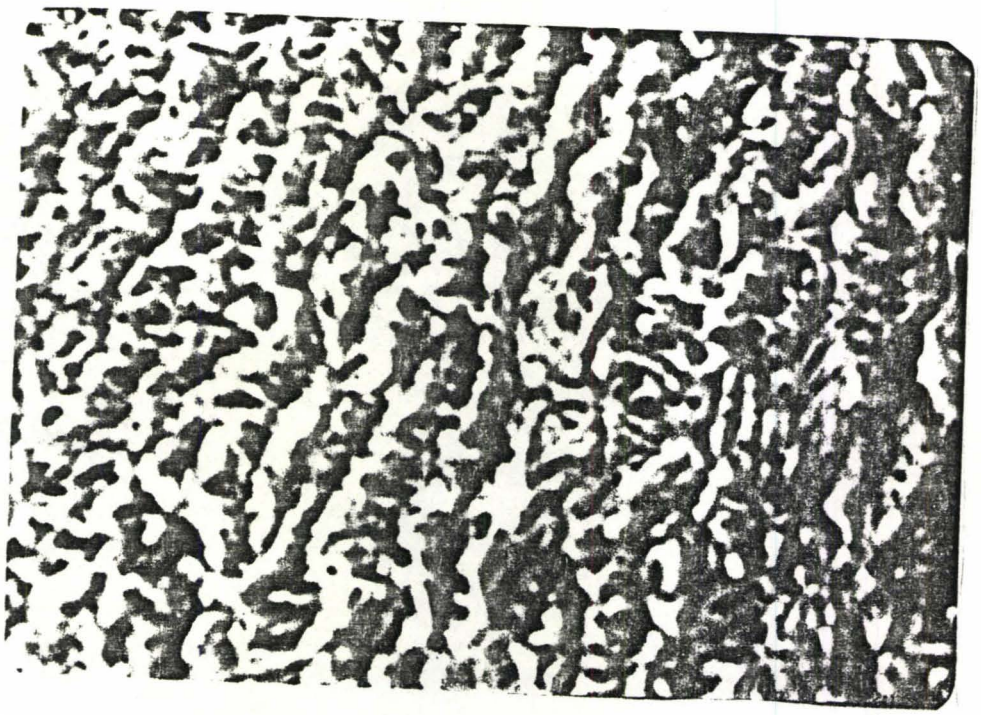

Fig. 11(k): Photocopy of Histological Micrograph of Native Abdominal Skin (Longitudinal Sample)

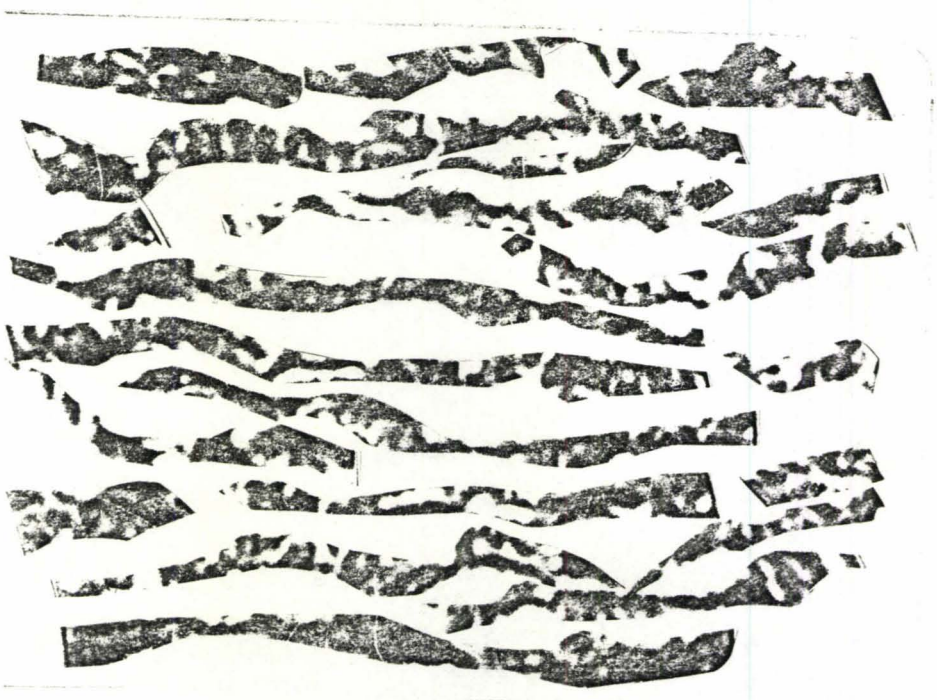

Fig. 11(l): Elastin Parts but Out from Fig. 11(k) Giving an Elastin Content of 23%

Fig. 12: Histological Micrograph of Decollagenated Achilles Tendon. Verhoeff's Stain (x400)

Fig. 13: Histological Micrograph of Decollagenated Cornea. Verhoeff's Stain (x400)

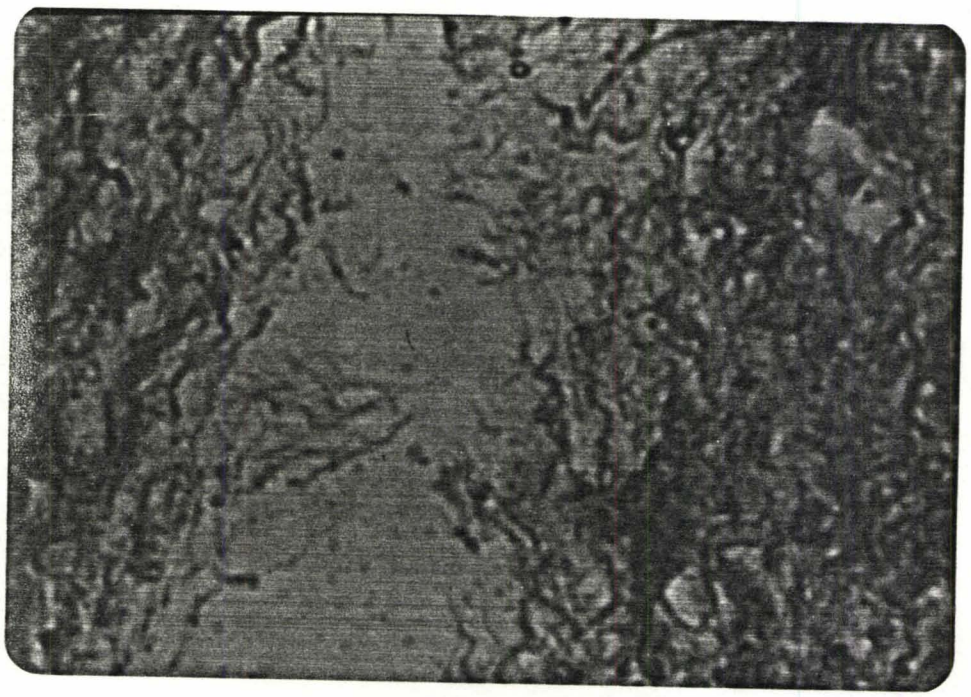

Fig. 14: Histological Micrograph of Decollagenated Sclera. Verhoeff's Stain (x400)

TISSUE	PERCENT MICROVOIDS	PERCENT MACROVOIDS (= % ELASTIN)	HISTOLOGY* (% ELASTIN)
Descending Aorta	7.59 ± 0.16	19.20 ± 0.35	20,23
Ascending Aorta	6.10 ± 0.50	14.90 ± 1.30	16,14
Achilles Tendon	2.90 ± 0.30	7.5 ± 1.10	0
Abdominal Skin	8.51 ± 0.75	26.50 ± 1.50	23,19
Cornea	10.50 ± 0.65	13.75 ± 1.90	0
Sclera	5.20 ± 0.90	12.20 ± 1.75	0

* See Text

TABLE 1: Computer and Histological Results for Elastin Content

Project I) and ignoring their standard deviations.

Before the correction is made, one needs to find out how the area of cross-section of the tissues samples change with elongation.

Experiments performed on three samples of native descending aorta show that the average change in the area of cross-section of these samples between the unstressed state and the stressed (ε = 100%) state was 50.0% (±2.0) as shown in Table 3. When these samples were deelastinated and the same measurements were performed, the average change in cross-sectional area was found to be 50.0% (±0.85) as in Table 3. All the descending aorta samples showed isovolumic behaviour, i.e. the volume of

the tissue remained unchanged with elongation, as evident from Table 3. This fact enables us to predict the change in cross-sectional area of the descending aorta tissue strip at any given extension. Although similar experiments are not done for the ascending aorta, it can be deduced that a similar isovolumic behaviour holds true for the ascending aorta as shown by Patel et. al. (10).

For the case of the Achilles tendon, the change in the cross-sectional area with elongation is negligible since the maximum strain attained was only 4%. This is in accordance with Abraham's (1) observation when he studied the mechanical behaviour of tendon in vitro. Similarly the same assumption can be made for the cornea and the sclera, since in both tissues the maximum strain attained was in the region of 20-25% only as shown in Project I.

For the abdominal skin, experiments performed on three samples of the native tissue in the longitudinal direction showed that the average change in the cross-sectional area of the tissue samples between the unstressed state and the stressed (ε = 160%) state was 65.67% (±4.04) as in Table 3; while the corresponding figure for the deelastinated tissues was 65.17% (±2.75) as shown in Table 3. Fig. 15 shows the appearance of the descending aorta at various extensions while being stretched by the tensile machine.

Now the high-strain moduli of the various tissues can be corrected for microvoid and macrovoids. These corrected moduli are shown in Table 2 together with the nominal moduli.

The corrected values of high-strain moduli in Table 2 are calcu-

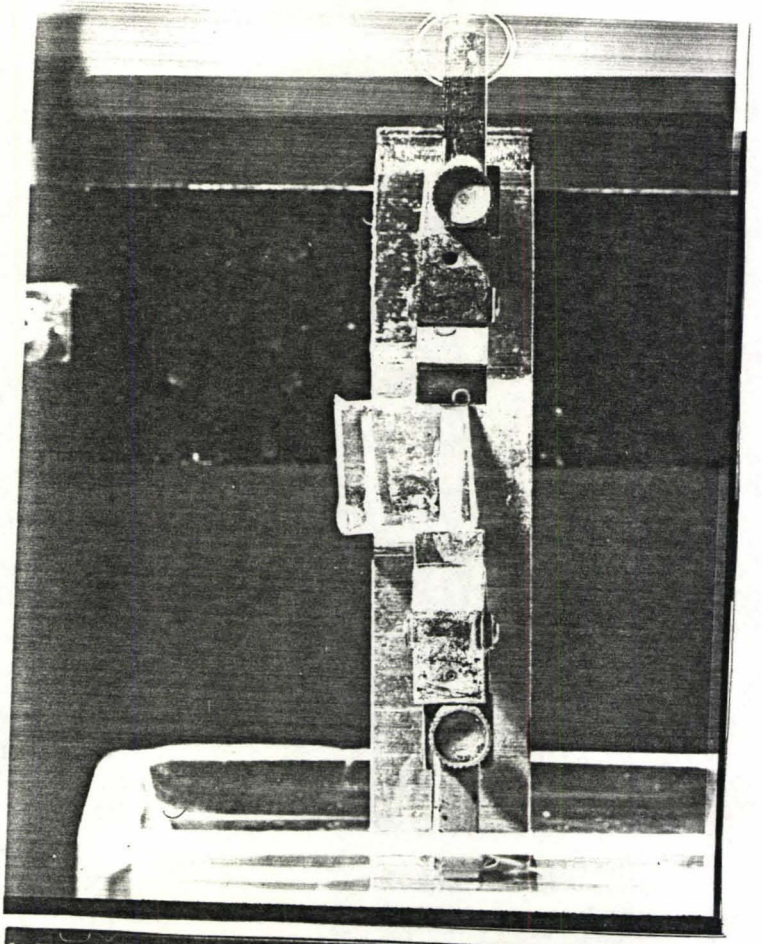

15(a)

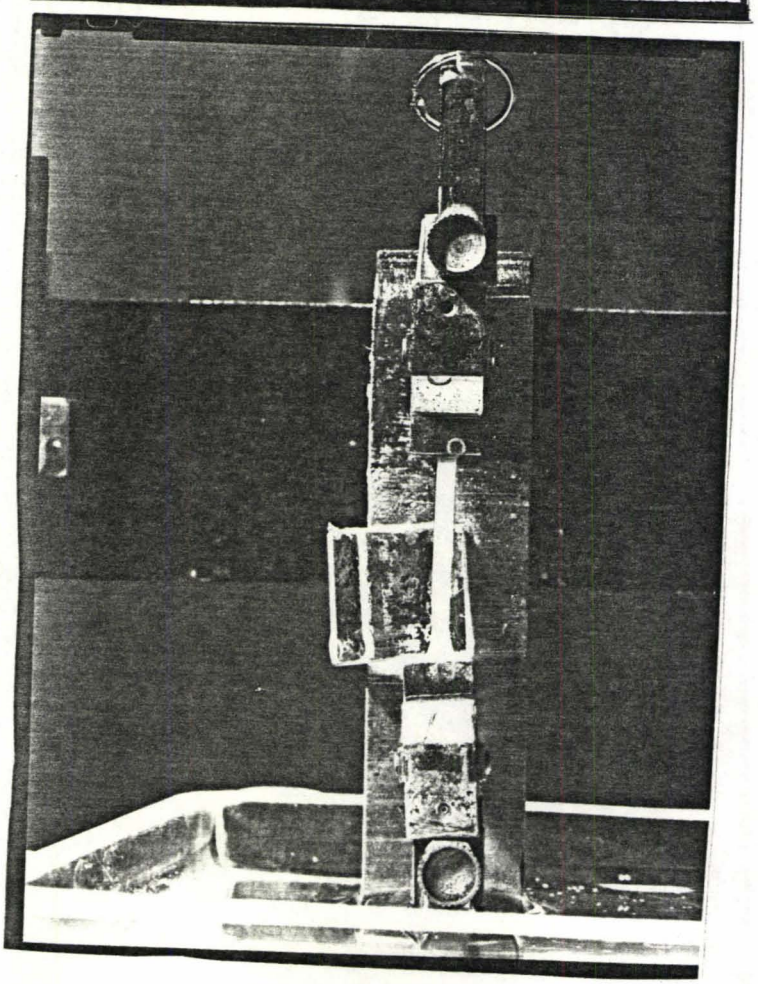

15(b)

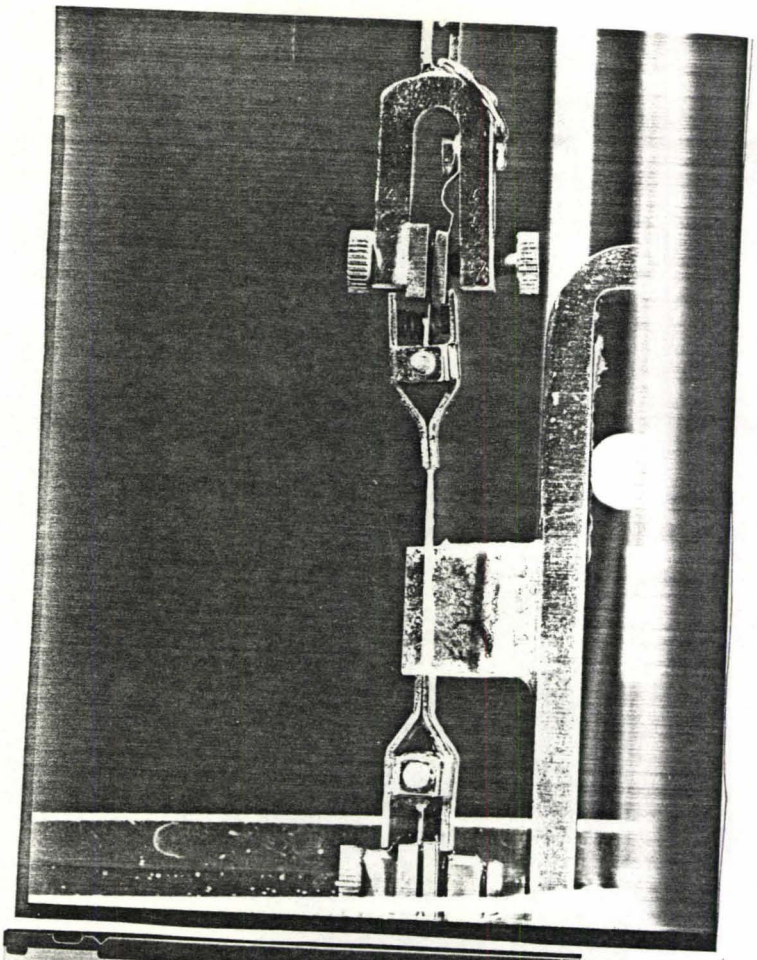

15(c)

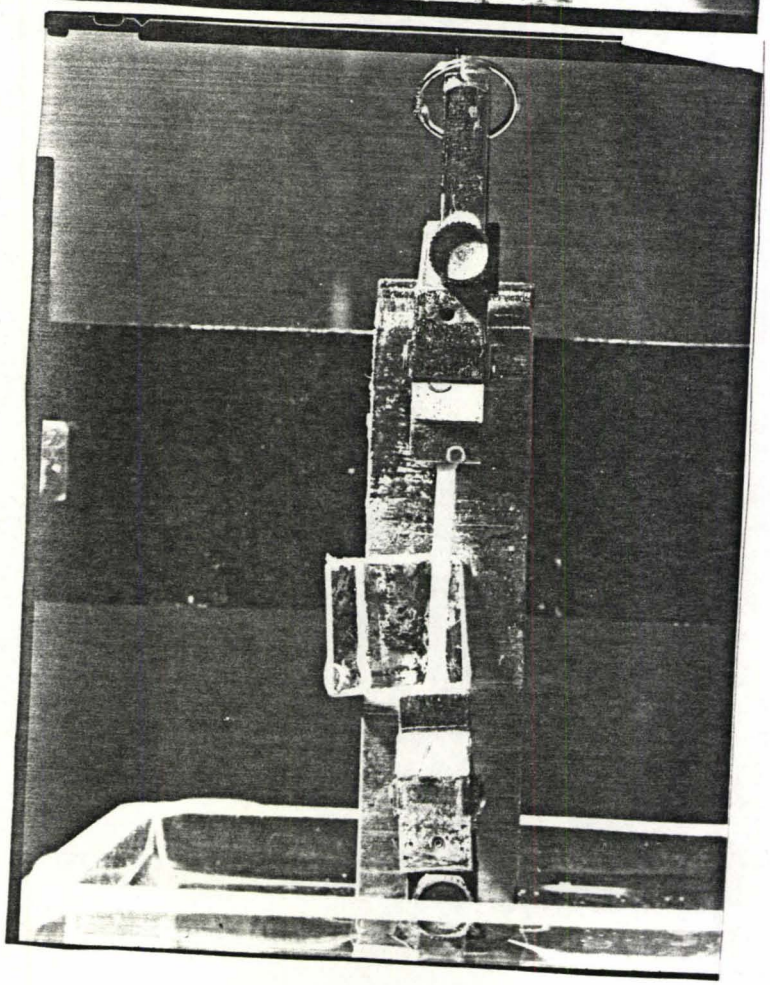

15(d)

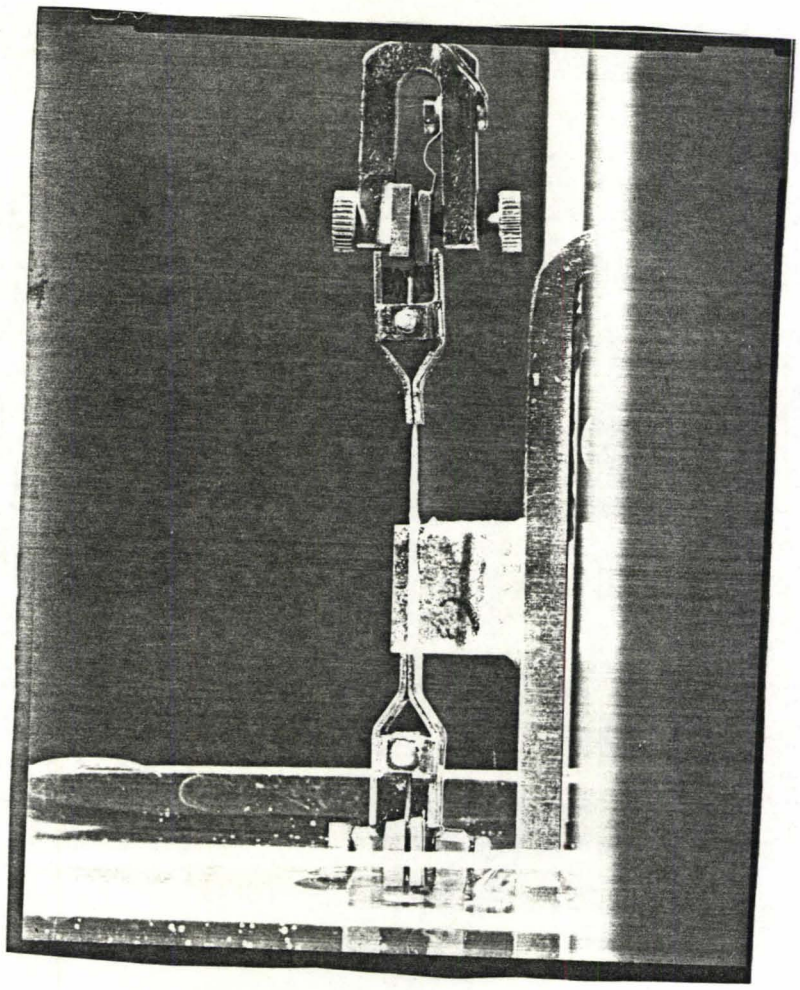

15(e)

Fig. 15: Photographs of Native Descending Aorta Tissue Strip Showing Isovolumic Behaviour on Extension

Fig. 15(a): shows length, width, and thickness of tissue strip in the unstressed state

Fig. 15(b): shows length, width and thickness at 62% strain

Fig. 15(c): shows length and thickness at 62% strain

Fig. 15(d): shows length, width, and thickness at 82% strain

Fig. 15(e): shows length and thickness at 82% strain

lated in the following manner. As an example the modulus of the descending aorta will be used to illustrate the method of calculation. As shown in Table 2 the nominal high-strain modulus of the native descending aorta in the circumferential direction is 737.8 gm/mm^2 and the percentage microvoids is 7.6%. The modulus of 737.8 gm/mm^2 is for 1 mm^2 of the tissue. Since the descending aorta has a microvoid content of 7.6%, the actual area of the tissue is 1-0.076 mm^2 or 0.924 mm^2. The corrected high-strain modulus for the native descending aorta is now 737.8/0.924 gm/mm^2 or 798.5 gm/mm^2 as shown in Table 2. For the deelastinated tissue both the microvoids and macrovoids have to be taken into account. The total void content in the deelastinated descending aorta is 7.6 + 19.2 = 26.8% as shown in Table 1. The nominal high-strain modulus of the deelastinated descending aorta in the circumferential direction is 790.2 gm/mm^2 as shown in Table 2. The actual area of the tissue is now 1-0.268 or 0.732 mm^2. Therefore the corrected high-strain modulus of the deelastinated descending aorta in the circumferential direction is now 790.2/0.732 or 1079.5 gm/mm^2 as shown in Table 2.

Once again referring to Table 3, it is evident that all the descending aorta samples show isovolumic behaviour. Similarly all the abdominal skin samples show isovolumic behaviour with the exception of sample #2 which shows a difference of 22% in the volume of the skin before and after stretching. So it can be concluded that both the aorta and the skin show isovolumic behaviour. This means that the area of cross-section of the tissue strip at any given extension can be determined provided one knows the original unstressed length, ℓ_o and the original unstressed cross-sectional area, A_o i.e. by means of the relation

$A_o \ell_o = A.\ell$ where A and ℓ are the area of cross-section and length of tissue strip at any extension. Using this isovolumic relationship and knowing the microvoid and macrovoid content of the tissue will enable one to correct for the modulus of the tissue at any extension.

Now the stress-strain curves for all the tissues can be corrected for microvoids and macrovoids. The typical corrected stress-strain curves together with the typical nominal curves are shown in Figs. 16 to 19 for the cases of the ascending aorta, descending aorta, abdominal skin and cornea.

Determination of MPS Content

By the dry weight technique of comparing the weights of the tissues before and after MPS removal the percentage of MPS in the ascending aorta, Achilles tendon, and cornea were found to be 6.19% (±1.10), 4.30% (±0.75), and 3.47% (±0.65) respectively; these being mean values (± standard deviation) for three samples of each tissue. Further, Figs. 8, 9, and 10 indicate that the porosity curves of these tissues before and after MPS removal are almost identical.

TISSUE	PERCENTAGE MICROVOIDS	PERCENTAGE MACROVOIDS	NATIVE		DEELASTINATED	
			HIGH ε MODULUS		HIGH ε MODULUS	
			nominal (gm/mm^2)	corrected (gm/mm^2)	nominal (gm/mm^2)	corrected (gm/mm^2)
Descending Aorta	7.6	19.2	737.8 (C.S.) 353.9 (L.S.)	798.5 383.0	790.2 (C.S.) 327.7 (L.S.)	1079.5 447.7
Ascending Aorta	6.1	14.9	98.68 (C.S.) 100.19 (L.S.)	105.1 106.7	64.31 (C.S.) 75.50 (L.S.)	81.4 95.6
Achilles Tendon	2.9	7.5	59368.0	61141.1	57815.0	64525.7
Abdominal Skin	8.5	26.5	1908.9 (T.S.) 1875.0 (L.S.)	2086.2 2049.2	1602.3 (T.S.) 2164.8 (L.S.)	2465.0 3330.5
Cornea	10.5	13.8	2953.4	3300.0	2537.5	3352.0
Sclera	5.2	12.2	5445.2	5743.9	4479.6	5423.2

C.S. = circumferential sample

L.S. = Longitudinal sample

T.S. = Transverse sample

TABLE 2: Corrected Values of High Strain Moduli of Dog's Tissues

Descending Aorta

	NATIVE						DEELASTINATED				
Sample #	Original unstressed length (ℓ_o)	Unstressed area (A_o)	area at ε = 10%	ΔA^*_{10}	area at ε = 100%	$\Delta A^\dagger_{100}$	Unstressed area (A_o)	area at ε = 10%	ΔA_{10}	area at ε = 100%	ΔA_{100}
1	10 mm	2.50 mm^2	2.35 mm^2	6.0%	1.20 mm^2	52.0%	2.65 mm^2	2.50 mm^2	5.7%	1.35 mm^2	49.1%
2	10 mm	2.15 mm^2	2.00 mm^2	7.0%	1.00 mm^2	50.0%	2.30 mm^2	2.16 mm^2	6.1%	1.15 mm^2	50.0%
3	10 mm	2.85 mm^2	2.70 mm^2	5.3%	1.40 mm^2	48.1%	3.05 mm^2	2.82 mm^2	7.5%	1.50 mm^2	50.8%

Abdominal Skin

	NATIVE						DEELASTINATED				
Sample #	Original unstressed length (ℓ_o)	Unstressed Area (A_o)	area at ε = 10%	ΔA_{10}	area at ε = 160%	+ ΔA_{160}	Unstressed area (A_o)	area at ε = 10%	ΔA_{10}	area at ε = 160%	ΔA_{160}
1	10 mm	2.80 mm^2	2.59 mm^2	7.5%	0.98 mm^2	65.0%	3.00 mm^2	2.67 mm^2	11.0%	0.96 mm^2	68.0%
2	10 mm	2.42 mm^2	2.21 mm^2	8.7%	0.73 mm^2	70.0%	2.60 mm^2	2.30 mm^2	11.5%	0.91 mm^2	65.0%
3	10 mm	2.50 mm^2	2.28 mm^2	8.8%	0.95 mm^2	62.0%	2.65 mm^2	2.33 mm^2	12.0%	1.00 mm^2	62.5%

$$* \Delta A_{10} = \frac{\text{unstressed area } (A_o) - (\text{area at } \varepsilon = 10\%)}{\text{unstressed area } (A_o)} \qquad \dagger \Delta A_{100} = \frac{\text{unstressed area } (A_o) - (\text{area at } \varepsilon = 100\%)}{\text{unstressed area } (A_o)}$$

$$+ \Delta A_{160} = \frac{\text{unstressed area } (A_o) - (\text{area at } \varepsilon = 160\%)}{\text{unstressed area } (A_o)}$$

TABLE 3: Reduction in Area with Elongation for Descending Aorta and Abdominal Skin

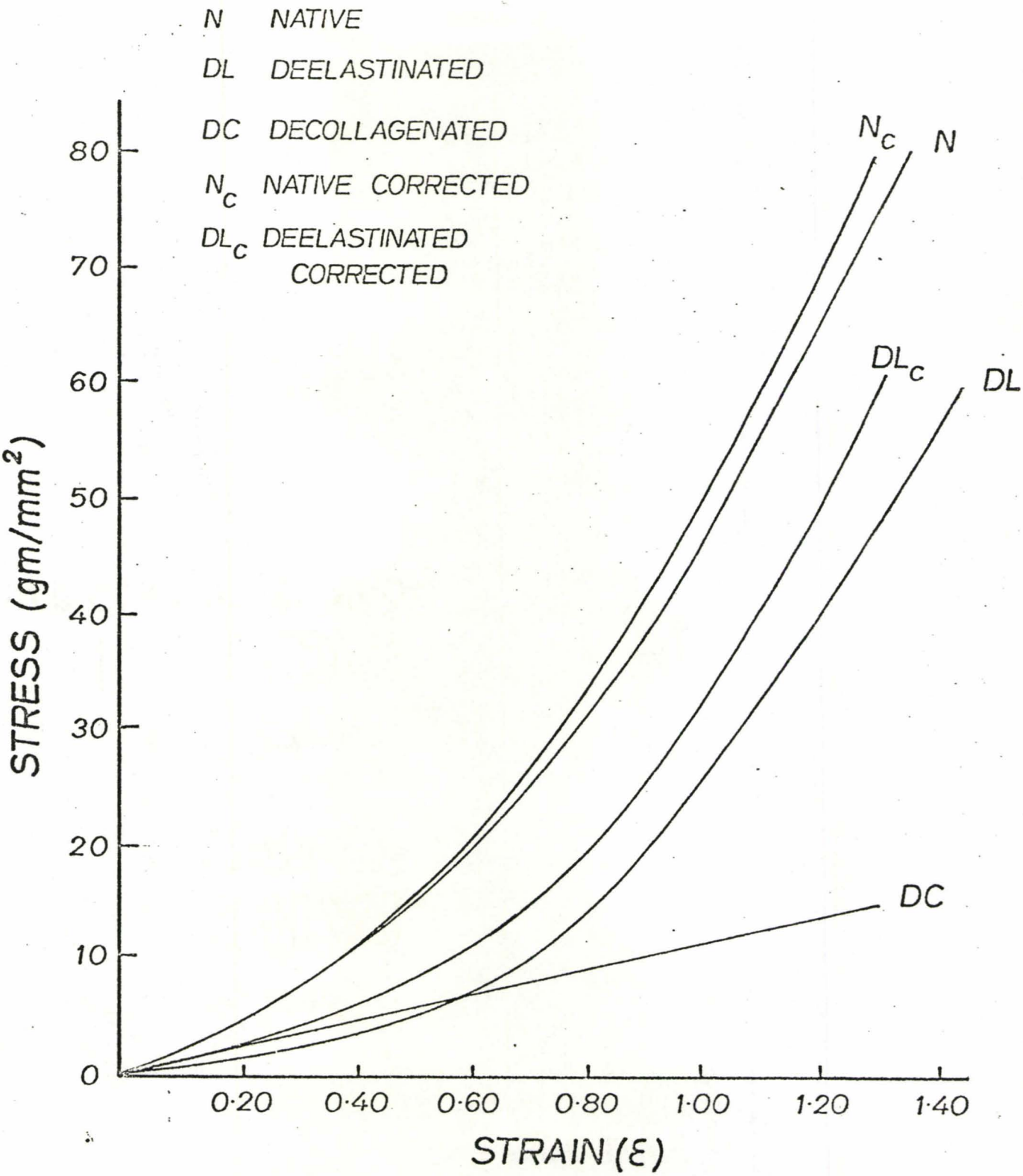

Fig. 16: Nominal and Corrected Stress-strain Curves for Ascending Aorta (Longitudinal Sample)

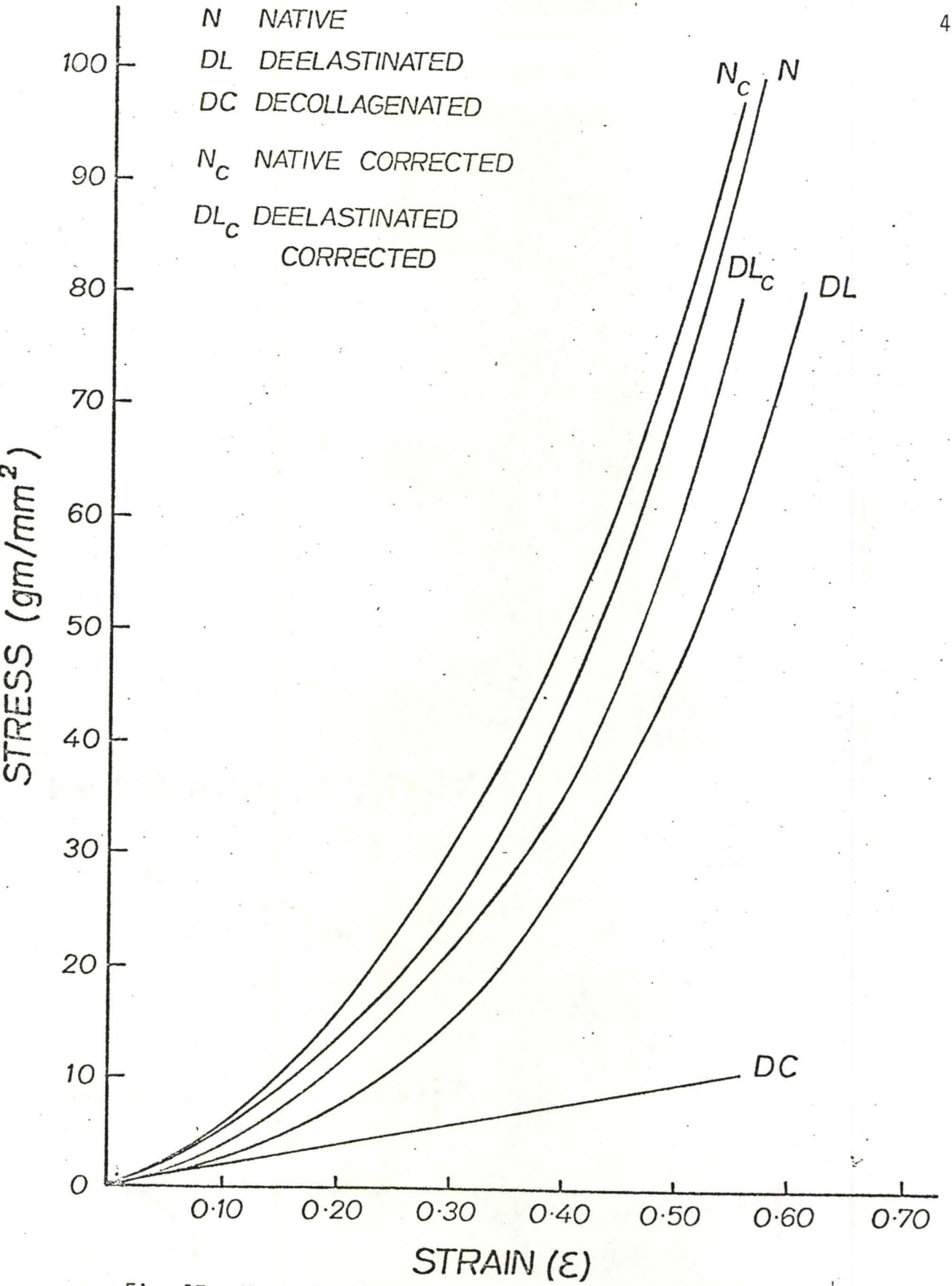

Fig. 17: Nominal and Corrected Stress-strain Curves for Descending Aorta (Longitudinal Sample)

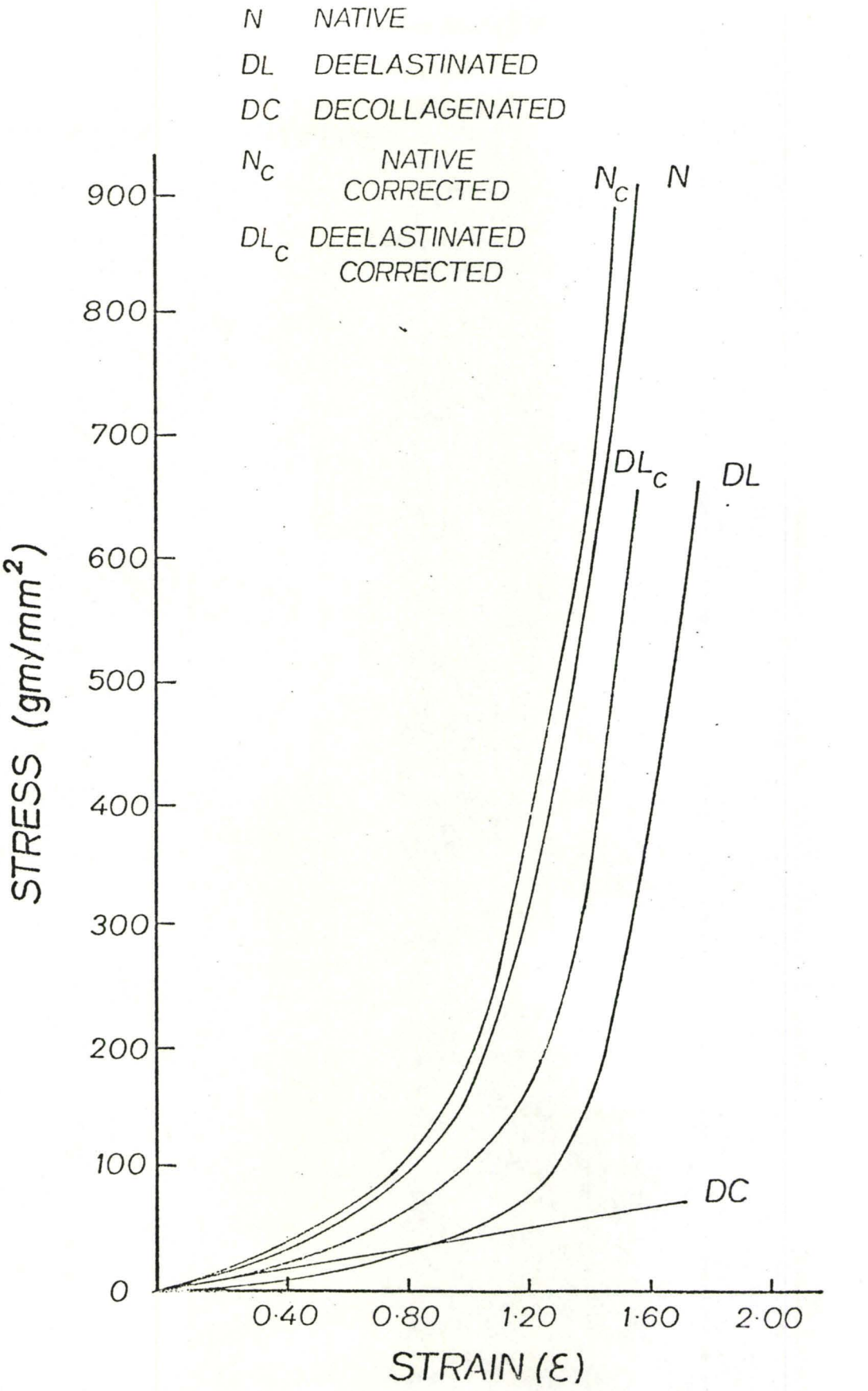

Fig. 18: Nominal and Corrected Stress-strain Curves for the Abdominal Skin (Transverse Sample)

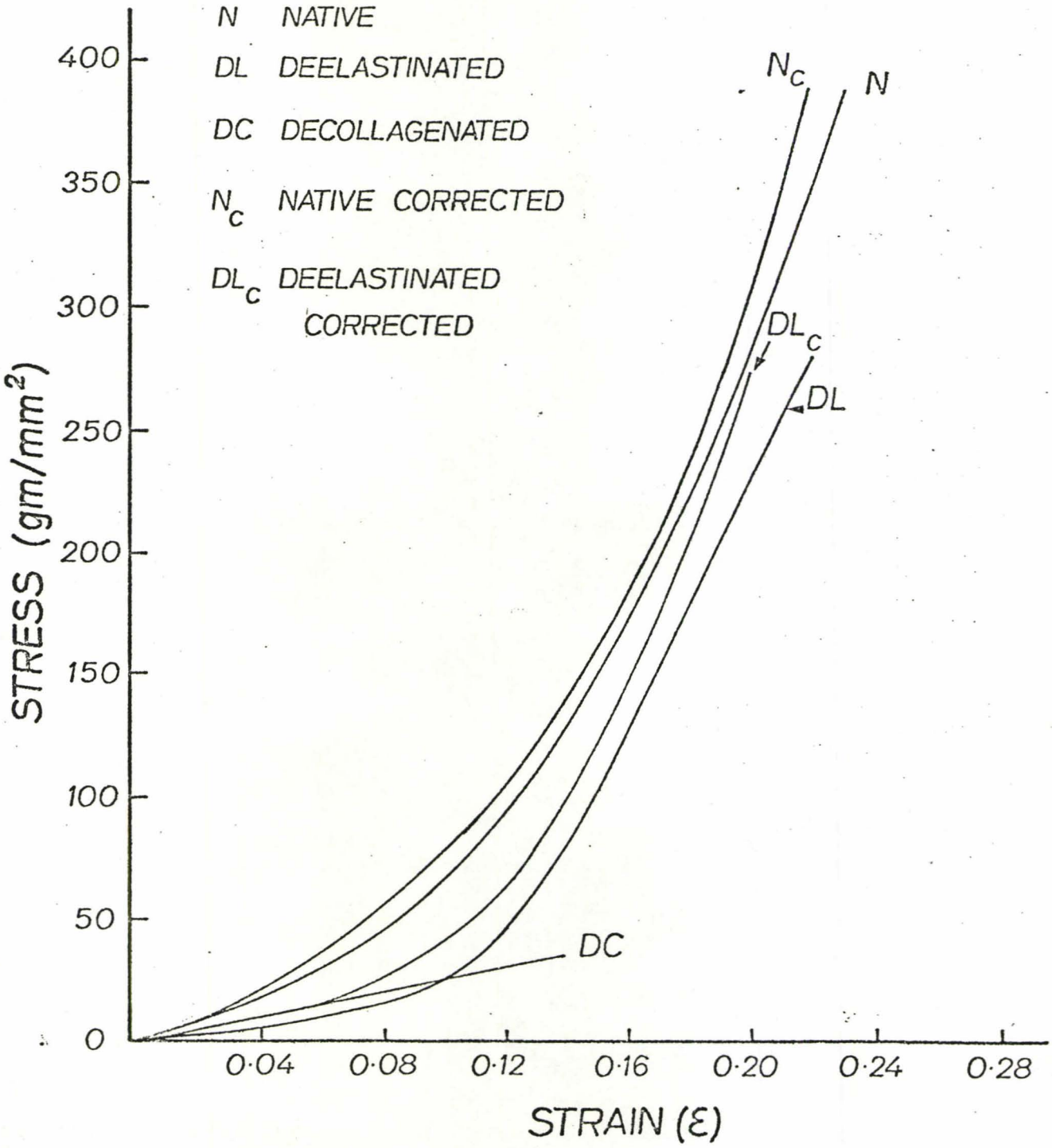

Fig. 19: Nominal and Corrected Stress-strain Curves for Ascending Aorta (Longitudinal Sample)

DISCUSSION

This discussion will take into account the results obtained in Project I as well.

Table 2 indicates that the area correction for microvoids is very important for the case of the abdominal skin due to its high microvoid content. It has also been shown earlier that there was an average change of 65.67% in the cross-sectional area between the unstressed native abdominal skin and the stressed (ε = 160%) skin. There was also an average change of 65.17% in the cross-sectional area between the unstressed deelastinated abdominal skin and the stressed (ε = 160%) deelastinated skin. These changes in cross-sectional area indicate isovolumic behaviour of the skin and this fact can be used to correct the modulus at any extension. As a result of the correction for microvoids, the high strain moduli of the native abdominal skin in both the longitudinal and transverse samples increased by about 9%. This indicates the importance of correcting for microvoids. Kenedi et. al. (5) observed a similar phenomenon of reduction in cross-sectional area with stretching when they studied human skin in vitro. They (5) defined "active" strain, ε_a, as increase in gauge length/unstrained gauge length; "passive" strain, ε_p, as decrease in width/unstrained width; and strain ratio K as $\varepsilon_p/\varepsilon_a$. Kenedi et. al. (5) found that the most significant and revealing feature of their uni-directional tensile tests on strips of native human skin was the variation of the strain ratio K as shown in Fig. 3 of (5). They (5) found the contraction in width with elongation to be considerable,

K rising to values in excess of 1.0 and this rise was particularly rapid in older skin. The reduction in cross-sectional area with stretching acquires meaning only when considered in relation to the histological structure of skin (5). This will be discussed further in the later part of this discussion.

The only other tissue in which the area correction for microvoids is essential is the cornea. The cornea indicates a microvoid content of 10.5% as shown in Table 2. As a result of this correction the high strain modulus of the cornea increased by 11%.

For all the other tissues, correction for microvoids is not essential since it does not change the high-strain moduli by more than 8%.

The area correction for voids in the deelastinated tissues is highly critical for all the tissues with the possible exception of the Achilles tendon.

Table 2 indicates a 19.2% (±0.35) percentage macrovoids (i.e. 19.2% elastin) for the descending aorta. As a result of the correction for microvoids and macrovoids the high strain moduli in both the longitudinal and circumferential samples of the deelastinated tissue increased by 37%. Lake (6) determined the elastin content of the bovine's upper descending thoracic aorta by a similar porosity technique and found the percentage elastin to be 23% which was confirmed by estimates of macrovoids from micrographs of histologic sections. In this report histological estimates of elastin from micrographs of native descending aorta were 20% and 23% (as shown in Table 1) giving an average value of 21.5%

elastin. Neuman and Logan (9) determined the collagen and elastin content in various mammalian tissues by a chemical method and found an elastin content of 39.8% in beef aortic arch and a corresponding figure of 53.4% in pig's aortic arch; these figures were based on dry fat-free weight. However, Neuman and Logan (9) did not confirm their results with histology.

The macropore diffusivity or diffusion coefficient, D_2, needed to fit the theoretical porosity curve to the experimental one is 0.315 x 10^{-5} cm^2/sec as compared to the tabulated molecular diffusivity of NaCℓ which is 1.5 x 10^{-5} cm^2/sec (6). This agreement is extremely good in view of Lake's (6) value of D_2 which was nearly 5 times the value of NaCℓ diffusivity. Similar comparisons do not exist for the micropore diffusivity, D_2 (6). This is because the micropore region is a continuum unlike other experimental work on the effect of pore size on solution diffusivities (6). Furthermore, a 19.2% elastin content in the descending aorta is reasonable in view of the extended initial "toe" of the stress-strain curve of the deelastinated descending aorta as shown in Project I. This extended initial "toe" is also apparent in the stress-strain curves of the dog's thoracic aorta as determined by Yamada (13) although he confined his studies to the native tissue only.

For the ascending aorta the average elastin content was found to be 14.90% (±1.30) as shown in Table 1; as a result of which the corrected high strain moduli of the deelastinated ascending aorta in both the circumferential and longitudinal direction increased by 27% as shown in Table 2. Histological estimates of elastin from micrographs of the

native ascending aorta were 16% and 14% giving an average value of 15% which is in good agreement with the data obtained from the porosity studies. Furthermore, a figure of 14.9% for the elastin content of the ascending aorta is reasonable since the stress-strain curves for both the native and deelastinated tissue showed an extended initial toe as shown in Project I. This has been confirmed indirectly by Yamada's observation (13) on the dog's ascending aorta where he reported an ultimate tensile strength of 70 gm/mm^2 and an ultimate percentage elongation of 145%, although Yamada (13) did not draw the actual stress-strain curve for the dog's ascending aorta. No direct comparison can be made for the elastin content of the dog's ascending aorta although Neuman and Logan (9) quoted a figure of 39.1% for the elastin content of beef aortic arch and 53.4% for the pig's aortic arch; these figures being based on dry fat-free weight (9).

For the abdominal skin, Table 1 indicates an elastin content of 26.5% (±1.50). After correcting for microvoids and macrovoids, the high strain moduli of the deelastinated abdominal skin in both the transverse and longitudinal samples were increased by 54% (Table 2). This difference in moduli is indeed tremendous due to the high elastin content (26.5%) in the abdominal skin (Table 1).

As reported ealier in this discussion, Kenedi et. al. (5) observed a reduction of cross-sectional area in native human skin with stretching and reported that this reduction in cross-sectional area of native skin strip with stretching can be explained in terms of the histological structure of skin (5). The load resistive part of this structure consists

of a criss-cross network of randomly intertwined collagen bundles as shown in the "Histology" section of Project I. Histological evidence showed that increasing load application produced increasing straightening and orientation of the collagen bundles in the direction of load or stress (as shown clearly in "Histology of Stretched Tissues" section of Project I) culminating in a fully oriented and virtually closely packed collagenous structure. Since the interbundle spaces are filled with tissue fluid this closure of the collagen bundle network must be accomplished in part against the resistance of this fluid (5). Further as the bundles approach each other it would be expected that tissue fluid will be squeezed out from the interspaces (5).

The elastin content of 26.5% in abdominal skin was confirmed by histological estimates to be 23% and 19% giving an average figure of 21% (Table 1). An elastin content of 26.5% in the abdominal skin is hardly surprising since the stress-strain curves for both the native and deelastinated skin in both the transverse and longitudinal directions show a very highly extended initial toe region as can be seen from the relevant curves in Project I. This phenomenon of a highly extended initial toe region for the stress-strain curves was also observed by Yamada (13) when he studied the mechanical properties of dog's abdominal skin. Kenedi et. al. (5) and Ridge and Wright (11) observed the same phenomenon when they studied human skin in vitro. Kenedi et. al. (5) also observed that the human abdominal skin in the direction of the longitudinal axis of the body was more extensible at low loads than the circumferential section. This phenomenon was evident from the stress-strain curves of native abdominal skin as reported in Project I.

Comparison of the elastin content of the dog's abdominal skin with previous work is rather difficult because of the scarcity of the relevant findings. The only work is that by Neuman and Logan (9) where they determined the collagen content of dog's skin and found it to be 64.5% based on dry fat-free weight.

The elastin content of the Achilles tendon was found, by porosity experiment, to be 7.5% (±1.10) as shown in Table 1. When the high strain modulus of the tendon was corrected for microvoids and macrovoids, the new modulus differed from the nominal value by 12% (see Table 2). This is relatively small increase in modulus as compared to the increase in the moduli of the deelastinated descending aorta (37%), deelastinated ascending aorta (27%), and deelastinated abdominal skin (54%) as shown in Table 2. The stress-strain curve of the deelastinated Achilles tendon when compared with the stress-strain curve of the native tendon indicated the presence of elastin (see Project I) and histology of the decollagenated tendon supported this observation (see Fig. 12). Elastin is not seen in the histology of the native tendon probably because of the dense and closely-packed collagenous network in the tissue masking the relatively meagre elastin. Hass (4) observed a similar phenomenon in the intimal plaque of the human aorta which in the intact aorta was composed principally of dense collagen bundles. On removal of the collagen by extraction, the residual structure of the sclerotic plaque persisted in the form of a system of delicate elastic networks as shown in Fig. 2 of (4). Also stress-strain curves of both the native and deelastinated Achilles tendon showed an extremely short "toe" region (see Project I) indicative of a low elastin content. Another possibility is that the action of elastase

even in the presence of trypsin inhibitor may have weakened or disorganized the reticular fibres or very young collagen fibres. Thus the appearance of elastin-like mechanical behaviour of the native tendon tissue may be due to reticular and not elastin fibres (or a mixture of both). A similar observation regarding the low elastin content was made by previous workers like Abrahams (1) who studied the stress-strain characteristics of human Achilles tendon, and found its elastic limit to be 4%, comparable to the elastic limit of the dog's Achilles tendon as reported in Project I.

The elastin content of the cornea was found to be 13.75% (±1.90) as shown in Table 1; and the corrected high strain modulus of the deelastinated tissue differed from the nominal modulus by 32%. The elastin content for the sclera was found to be 12.20% (±1.75) and the corrected high-strain modulus of the deelastinated sclera differed from the nominal value by 21%. In both the cornea and the sclera the stress-strain curves of the deelastinated tissues indicated the presence of elastin and histology of the decollagenated tissues support these observations (Figs. 13 and 14). Once again, the explanation for the absence of elastin in the histology of the native tissues lies in the way the collagen fibre bundles are arranged in these tissues. The dense collagen bundles in these tissues (see the relevant histology in Project I) masked and obscured the relatively fine elastic fibres as reported by Hass (4) when he observed a similar pheonomenon in the human aorta. Furthermore, the cornea and the sclera are multilayered tissues and therefore the histology depends on the layer considered.

For all the tissues the macropore diffusivity needed to fit the theoretical porosity curves to the experimental ones were less than the

tabulated molecular diffusivity of NaCℓ which is 1.5 x 10^{-5} cm^2/sec (6) but no comparison can be made with published data except possibly in the case of the descending aorta where the D_2 value was compared with the D_2 value obtained by Lake (6) where he determined the percentage macropore in bovine's upper descending thoracic aorta.

The corrected stress-strain curves (Figs. 16-19) show a shift to the left of the nominal curves. The corrected stress-strain curves for the native tissues are almost identical to the nominal curves except in the case of the abdominal skin and the cornea. In the case of the abdominal skin a correction has to be made for the rather high microvoids content of about 8%. In the case of the cornea the microvoid content was high (10.5%) resulting in a slightly different corrected stress-strain curve as compared to the nominal curve. The corrected stress-strain curves for the deelastinated tissues are different from the nominal deelastinated curves due to the corrections made for both the microvoids and macrovoids. Furthermore, from porosity measurements, all the tissues, except the Achilles tendon, were found to have high elastin content; (the highest being found in the abdominal skin) which explains the difference between the corrected and the nominal curves for the deelastinated tissues.

The porosity curves of the ascending aorta, the Achilles tendon, and the cornea before and after MPS removal were found to be almost identical as shown in Figs. 8-10. By the dry weight technique of comparing weights of tissues before and after MPS removal, the percentage of MPS in the ascending aorta, Achilles tendon, and cornea were found to be 6.19%, 4.30%, and 3.47% respectively, these being average values. From Project I it was shown that the MPS did not affect the stress-strain characteristics

of these three tissues. It can therefore be concluded here that the MPS serve only as a background substance or matrix in which all the other tissue constituents are embedded.

Table 2 shows the corrected moduli of the various tissues in the native and deelastinated states. The corrections for microvoids and macrovoids were based on the assumption that the voids are uniformly distributed through out the whole tissue samples. It has also been shown in Table 3 that the descending aorta and the abdominal skin exhibit isovolumic behaviour i.e. the volume of the tissue before stretching is equal to its volume at any given extension. Mathematically, it can be written as $A_o \ell_o = A.\ell$ where A_o is the original unstressed area, ℓ_o is the original length, A and ℓ are the area and length respectively at any given extension. Based on this relationship the modulus of the tissue at any extension or strain can be corrected if the microvoids and macrovoids content are known. It can be inferred that the ascending aorta would exhibit isovolumic behaviour too as verified by Patel et. al. (10).

Table 2 indicates a large variation in the corrected values of the high-strain moduli (i.e. collagen moduli) of the various tissues; the highest modulus being found in the Achilles tendon and it is in the region of 60 kg/mm^2. As explained in Project I, the variation could be due to variation of the cohesion between the collagen fibres, to variation of the molecular orientation within the tissues, to some variation of the interweaving of the fibres, as explained by Elliott (2) for the case of the tendon. Elliott (2) further commented that expressed in terms of the collagen present, tensile strength ranges from 15-30 kg/mm^2 to 1-5 kg/mm^2 for the uterus and other tissues, "a discrepancy which seems too great to

be due to the orientation of the fibres and which implies a difference in the ultimate links of the collagen network" (2,3). In consequence it is rational to say that, it is the network disposition, form and interconnection of the collagen bundles that governs deformation rather than the characteristics of the collagen "material" itself (5). Ancillary to this the characteristics of the tissue fluid contained in the interbundle spaces, as in the case of skin, may have some influence and may be concerned in the differences shown by normal and aged or diseased tissue (5).

The stress-strain characteristics, histology, and porosity stuides (and hence determination of voids) are some of the parameters required for the proper designing of prosthetic devices. This is just a small part of the design criteria - much more work needs to be done. For instance, it is essential to know the chemical properties of tissues in terms of their interaction with body fluids. Creep and stress-relaxation studies have to be done to determine the degree of elastic recovery of the tissues. *In vivo* studies of the mechanical properties of the tissues are equally important. Patel *et. al.* (10) made a study of the static anisotropic elasticity in the middle descending thoracic aorta of 14 living dogs. Special transducers were used to measure radius and longitudinal stress at several pressures *in situ* in an isolated vessel segment. From these data, moduli describing elastic properties of the vessel wall were calculated. Their (10) results indicate that at a physiologic pressure of 154 cm H_2O (extension ratio of 1.52 circumferentially) the mean values for the incremental elastic moduli in the radial, circumferential, and longitudinal directions were 54.80, 75.10, and 101.0 gm/mm^2, respectively; these moduli increased with an increase in intravascular pressure and the

longitudinal modulus decreased by 32% when the vessel was studied *in vitro* due to the loss of longitudinal tethering (10). Kenedi *et. al.* (5) also carried out tests *in situ* on live human skin. The equipment used was a dynamometer to apply and measure load. The four arms of the dynamometer carry electrical resistance strain gauged steel plates to which, in the case of theatre work, stitches, directly anchored in the skin at the desired points of load application were attached. The load-strain curve on a detatched specimen of skin in longitudinal direction was compared with the curve obtained before removal of specimen of the skin from the back of the hand (Fig. 9 of (5)). They found that the results obtained from the comparable *in situ* and detached specimen tests showed good agreement and were correlatable as shown in Fig. 9 of (5).

The significance of this work on the stress-strain characteristics, histology, and porosity studies on dog's tissues lies in the fact that it serves as a foundation for the design of prosthetic devices and may also be useful in homograft and heterograft work. As reported earlier the elastin content of a tissue may also be a good indication of its pathological condition (7, 8, 12). These include observations of a rise in incremental Young's modulus with aging (7), possibly caused by an increase in the ratio of collagen to elastin fibres (8); and a general deterioration in the quality of intra-arterial components in vessels affected by arteriosclerosis (8).

SUMMARY OF CONCLUSIONS

1. By means of the porosity curves and the diffusion equations the elastin content of the various tissues from the dog was determined.
2. The figures for elastin content were supported, to some extent, by histology.
3. The area correction for microvoids is essential for the native abdominal skin and the native cornea. For the deelastinated tissues, correction for microvoids and macrovoids is essential for all the tissues studied except the Achilles tendon since its elastin content was found to be relatively low.
4. The removal of mucopolysaccharides (MPS) does not affect the porosity curves of the ascending aorta, Achilles tendon, and cornea.

REFERENCES

1. Abrahams, M., "Mechanical Behaviour of Tendon in Vitro. A Preliminary Report". Med. and Biol. Engng., 5, pp. 433-443, 1967.
2. Elliott, D.H., "Structure and Function of Mammalian Tendon". Biol. Rev., 40, pp. 392-421, 1965.
3. Harkness, R.D., "Biological Functions of Collagen". Biol. Rev., 36, pp. 399-463 1966.
4. Hass, G.M., "Elastic Tissue I: Description of a Method for the Isolation of Elastic Tissue". Archives of Pathology, 34, pp. 807-819 1942.
5. Kenedi, R.M.; Gibson, T.; and Daly, C.H., "Bio-Engineering Studies of Human Skin II". "Biomechanics and Related Bioengineering Topics. Proceedings of a Symposium Held in Glasgow, Sept., 1964". Ed. by R.M. Kenedi, Pergamon Press, London, 1965.
6. Lake, Larry W., "Structure-Property Relations of the Aortic Wall and its Tissue Constituents. Ph.D. Thesis, Rice University, 1973.
7. Learoyd, B.M., and Taylor, M.G., "Alterations with Age in the Viscoelastic Properties of Human Arterial Walls". Circulation Research, XVIII, pp. 278-292, 1966.
8. Mack, G., et. al., "Aortic Aging and Its Connection with Arteriosclerosis, Experimental Results". Journal of Cardiovascular Surgery (Torino), 11, pp. 292-296, 1968.
9. Neuman, Robert E.; and Logan, Milar A., "The Determination of Collagen and Elastin in Tissues". Journal of Biological Chemistry, 186, pp. 549-556, 1950.

10. Patel, Dali J.; Janicki, Joseph S.; and Carew, Thomas E., "Static Anisotropic Elastic Properties of the Aorta in Living Dogs". Circulation Research, XXV, pp. 765-779, 1969.

11. Ridge, M.D., and Wright, V., "The Directional Effects of Skin". Journal of Investigative Dermatology, 46, pp. 341-346, 1966.

12. Sumner, D.S.; Hokanson, D.E.; and Strandess, D.E., "Stress-Strain Characteristics and Collagen/Elastin Content of Abdominal Aortic Aneurysms". Surgery, Gynecology and Obstetrics, 130, pp. 459-466, 1970.

13. Yamada, Hiroshi, Strength of Biological Materials, Robert E. Krieger Publishing Company, Huntington, New York: 1973 (Ed. by F. Gaynor Evans).

APPENDIX

As shown before equation (38) will be solved by computer to find the volume of microvoids (V_1) and the volume of macrovoids (V_2). Reviewing Eq. 38

$$C_{ext}(t) = \frac{C_o V_2}{V_s}\left[1 - e^{-(\pi/2\ell)^2 D_2 t}\right] + \frac{C_o V_1}{V_s}\left[1 - e^{-(\pi/2\ell)^2 D_1 t}\right] \quad (39)$$

where $C_{ext}(t)$ = external concentration of saline in deionised water as calculated by the computer program and designated as ZZ (in moles/100 ml x 10^6),

C_o = concentration of saline in which the tissue samples are equilibrated before porosity expt. (= 0.01 mole/100 ml),

V_2 = volume of macrovoids in ml.,

V_1 = volume of microvoids in ml.,

V_s = volume of deionised water used = 100 ml.,

D_1 = diffusion coefficient due to microvoids, mm^2/sec.,

D_2 = diffusion coefficient due to macrovoids, mm^2/sec.,

t = time in sec.,

2ℓ = thickness of tissue in mm.

In the computer program output,

Z(J,I) = experimental value of C_{ext} in moles/100 ml. x 10^6,

ZZ(J,I) = computer value of C_{ext} in moles/100 ml x 10^6,

A(J) = $\frac{C_o V_2}{V_s}$, from which V_2 can be calculated since V_s and C_o are constants,

$B(J) = \frac{C_o V_1}{V_s}$, from which V_1 can be calculated,

T(J,I) = time in seconds.

In the program the following symbols are used:

NPE = number of points in each porosity experiment

NE = number of experiments

C(1) = Initial value of diffusion coefficient, D_1,

D(1) = Initial value of diffusion coefficient, D_2,

L(J) = value of $\pi/2\ell$

The input to the program are values of time and the corresponding $C_{ext's}$, initial values of D_1 and D_2 found by trial and error, NPE, NE and L(J). By the method of "least square fitting" the program computes the best fit values of C_{ext} (i.e. ZZ) together with the corresponding times, as well as A(J) and B(J); from the last two of which macrovoid and microvoid volumes can be calculated.

The principle of the Least Square Fitting is as follows:

Equation (39) is rewritten as

$$Z = AX + BY \qquad \text{(i)}$$

$$\sum X_i Z_i = A\sum X_i^2 + B\sum Y_i X_i \qquad \text{(ii)}$$

and $$\sum Y_i Z_i = A\sum X_i Y_i + B\sum Y_i^2 \qquad \text{(iii)}$$

Also $$\sum X_i Z_i \sum X_i Y_i = A\sum X_i^2 \sum X_i Y_i + B(\sum X_i Y_i)^2 \qquad \text{(iv)}$$

and $$-\sum Y_i Z_i \sum X_i^2 = -A\sum X_i^2 \sum X_i Y_i - B\sum X_i^2 \sum Y_i^2 \qquad \text{(v)}$$

Adding (iv) and (v) we have

$$\sum X_i Z_i \sum X_i Y_i - \sum Y_i Z_i \sum X_i^2 = B[(\sum X_i Y_i)^2 - \sum X_i^2 \sum Y_i^2]$$

i.e. $$B = \frac{\sum X_i Z_i \sum X_i Y_i - \sum Y_i Z_i \sum X_i^2}{[(\sum X_i Y_i)^2 - \sum X_i^2 \sum Y_i^2}$$

i.e. $$B = \frac{\sum Y_i Z_i \sum X_i^2 - \sum X_i Z_i \sum X_i Y_i}{\sum X_i^2 \sum Y_i^2 - (\sum X_i Y_i)^2} \qquad \text{(vi)}$$

$$\sum X_i Z_i \sum Y_i^2 = A \sum X_i^2 \sum Y_i^2 + B \sum Y_i X_i \sum Y_i^2 \qquad \text{(vii)}$$

$$-\sum Y_i Z_i \sum Y_i X_i = -A(\sum X_i Y_i)^2 - B \sum Y_i^2 \sum Y_i X_i \qquad \text{(viii)}$$

Adding (vii) and (viii)

$$\sum X_i Z_i \sum Y_i^2 - \sum Y_i Z_i \sum Y_i X_i = A[\sum X_i^2 \sum Y_i^2 - (\sum X_i Y_i)^2]$$

i.e. $$A = \frac{\sum X_i Z_i \sum Y_i^2 - \sum Y_i Z_i \sum Y_i X_i}{\sum X_i^2 \sum Y_i^2 - (\sum X_i Y_i)^2} \qquad \text{(ix)}$$

In the program the following symbols were used:

$\sum Y_i Z_i$ = SYZ in the program

$\sum X_i^2$ = SX2 in the program

$\sum X_i Z_i$ = SXZ in the program

$\sum X_i Y_i$ = SXY in the program

$\sum Y_i^2$ = SY2 in the program

FLOW CHART FOR COMPUTER PROGRAM

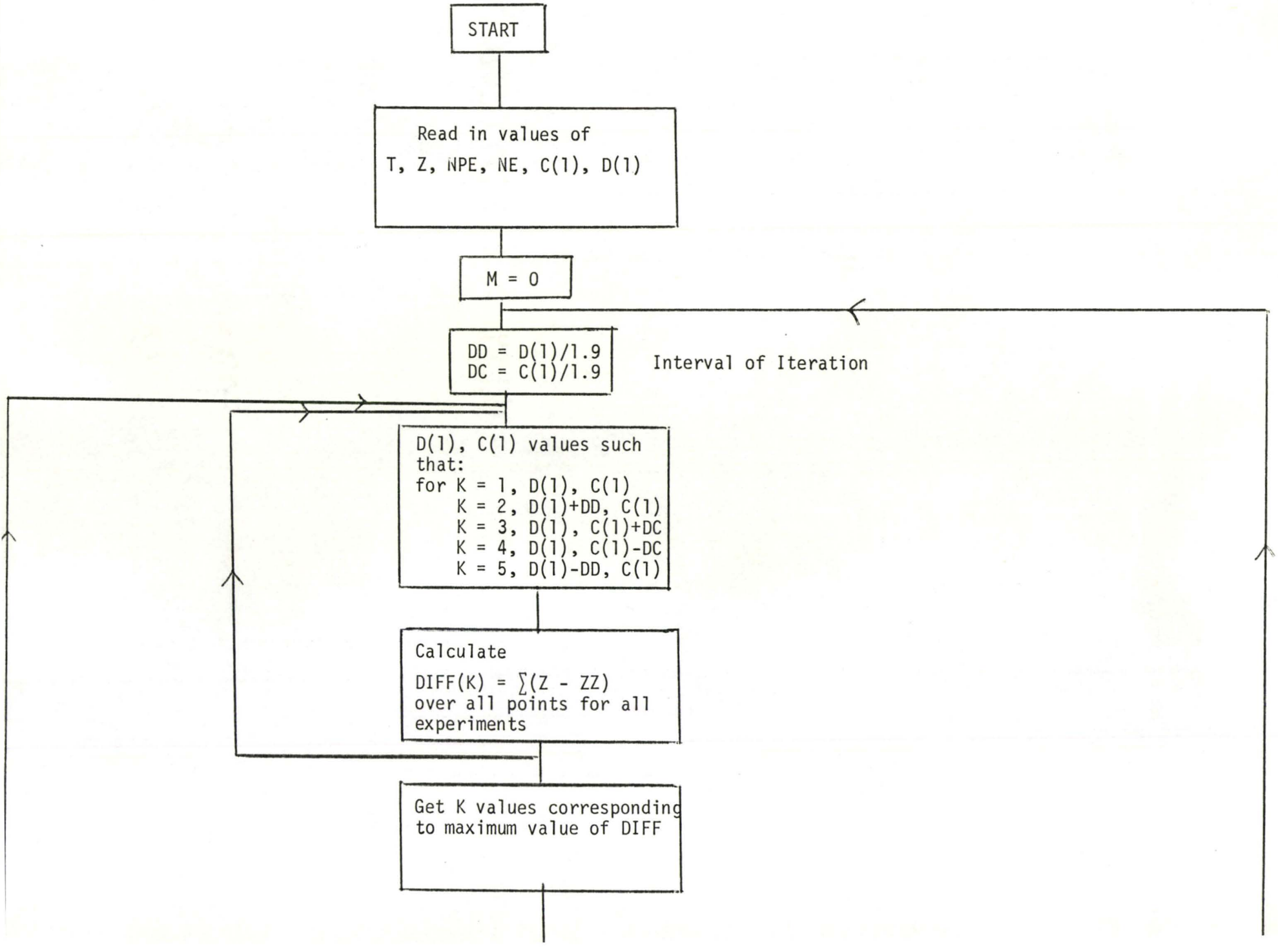

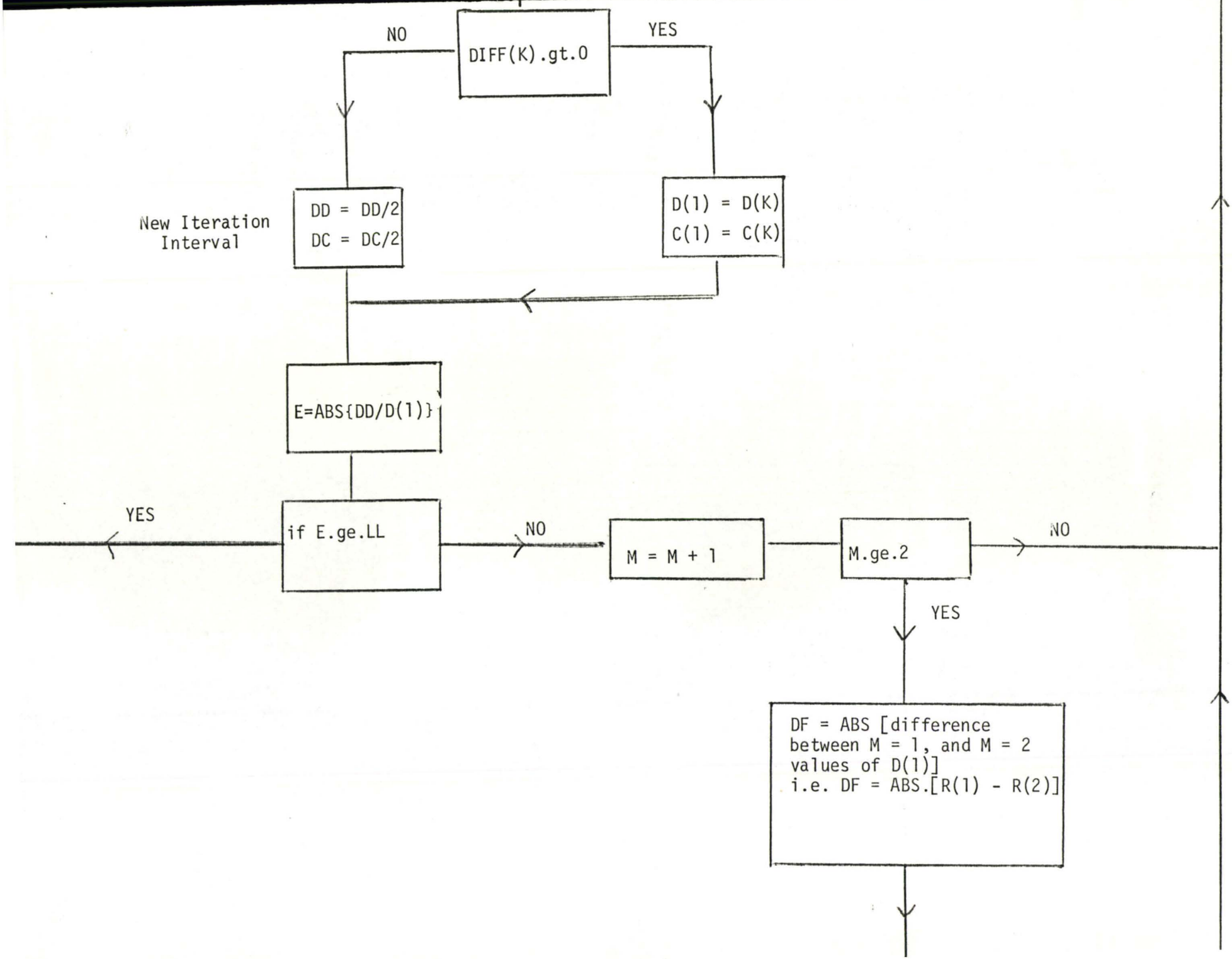
DIFF(K).gt.0
NO
YES
New Iteration Interval
DD = DD/2
DC = DC/2
D(1) = D(K)
C(1) = C(K)
E=ABS{DD/D(1)}
YES
if E.ge.LL
NO
M = M + 1
M.ge.2
NO
YES
DF = ABS [difference between M = 1, and M = 2 values of D(1)]
i.e. DF = ABS.[R(1) - R(2)]

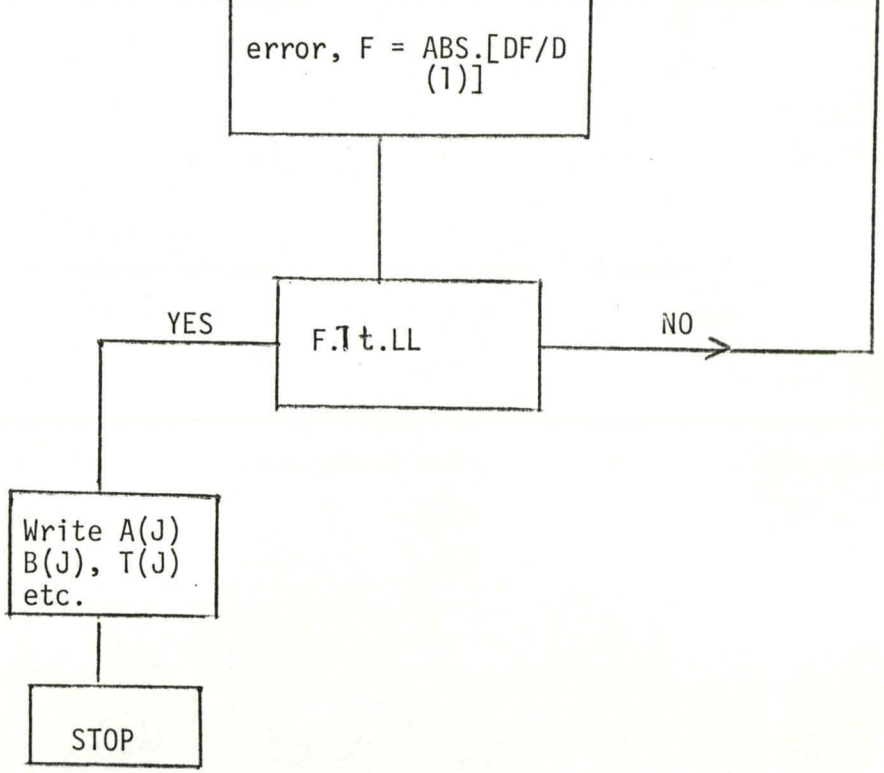

LEGEND

gt. = greater than
ge. = greater than or equal to
lt. = less than

```
      PROGRAM TSI (INPUT,OUTPUT,TAPE5=INPUT,TAPE6=OUTPUT)
      REAL SCI(5), DIFF(5), C(5), D(5), LL, B(2)
      REAL T(35,25),ZZ(35,25),X(35,25),Y(35,25),A(35),B(35)
      REAL Z(35,25),L(35)
   11 FORMAT(I4, I4, F8.5, F8.5, F8.5)
   22 FORMAT(F8.5)
   33 FORMAT(5(F6.1,F10.3))
   44 FORMAT(8X,*J*,16X,*I*,14X,*A(J)*,13X,*B(J)*,12X,*T(J,I)*,11X,*Z(J
     2,I)*,11X,*ZZ(J,I)*,///)
   55 FORMAT(07X,I2,15X,I2,11X,E10.3,7X,E10.3,9X,F6.1,9X,E10.3,7X,E10.3)
   66 FORMAT(*1*,17X,I2,5X,*EXPERIMENTS,*,5X,I2,5X,*POINTS IN EACH EXPER
     2IMENT,*,5X,*PRECISION IS *,F8.5)
   77 FORMAT(///,34X,*C = *,E10.3,25X,*D = *,E10.3,///)
   88 FORMAT(///,55X,*SCT = *,E10.3)
   99 FORMAT (*1*,10X,*D*,19X,*C*,18X,*DD*,18X,*DC*,18X,*SCT*,18X,*E*)
  111 FORMAT (5X,6(E10.3,10X))
      M = 0
      READ(5,11) NPE, NE, C(1), D(1), LL
      DO 21 J = 1,NE
      READ(5,22) L(J)
      READ(5,33) (T(J,I), Z(J,I), I=1,NPE)
   21 CONTINUE
      WRITE (6,99)
  310 DD = D(1)/1.9
      DC = C(1)/1.9
  270 K = 1
  110 SCT(K) = 0
      DO 31 J = 1,NE
      SY2 = 0
      SZX = 0
      SZY = 0
      SYX = 0
      SX2 = 0
      DO 41 I = 1, NPE
      X(J,I)=1.-EXP(-(L(J)*D(K)*T(J,I)))
      Y(J,I)=1.-EXP(-(L(J)*C(K)*T(J,I)))
      SY2 = SY2 + Y(J,I)**2
      SZX = SZX + Z(J,I)*X(J,I)
      SZY = SZY + Z(J,I)*Y(J,I)
      SYX = SYX + Y(J,I)*X(J,I)
   41 SX2 = SX2 + X(J,I)**2
      A(J) = (SY2 * SZX - SZY * SYX) / (SY2 * SX2 - SYX**2)
      B(J) = (SX2 * SZY - SZX * SYX) / (SY2 * SX2 - SYX**2)
      SC = 0
      DO 51 I = 1,NPE
      ZZ(J,I) = A(J) * X(J,I) + B(J) * Y(J,I)
   51 SC = (Z(J,I) - ZZ(J,I))**2 + SC
   31 SCT(K) = SC + SCT(K)
      DIFF(K) = SCT(1) - SCT(K)
   50 K = K + 1
      IF(K-3) 50, 60, 70
   50 D(2) = D(1) + DD
      C(2) = C(1)
      GO TO 110
   60 D(3) = D(1)
      C(3) = C(1) + DC
      GO TO 110
```

```
                  70    IF(K-5) 80, 9?, 100
                  80    D(4) = D(1)
60                      C(4) = C(1) - DC
                        GO TO 110
                  90    D(5) = D(1) - DD
                        C(5) = C(1)
                        GO TO 110
65                100   IF(DIFF(2) - DIFF(3)) 120, 120, 130
                  120   IF(DIFF(4) - DIFF(5)) 140, 140, 150
                  140   IF(DIFF(5) - DIFF(3)) 160, 160, 170
                  160   K = 3
                        GO TO 220
70                170   K = 5
                        GO TO 220
                  150   IF(DIFF(4) - DIFF(3)) 160, 160, 180
                  180   K = 4
                        GO TO 220
75                190   IF(DIFF(4) - DIFF(5)) 190, 190, 200
                  200   IF(DIFF(5) - DIFF(2)) 210, 210, 170
                  210   K = 2
                        GO TO 220
                  220   IF(DIFF(4) - DIFF(3)) 210, 210, 180
80                230   IF(DIFF(5)) 230, 230, 240
                        DD = DD/2
                        DC = DC/2
                      GO TO 250
                  240   D(I) = D(K)
85                      C(I) = C(K)
                  250   E=((DD/D(I))**2)**0.5
                        WRITE(6,11) D(K),C(K),DD,DC,SCT(K),E
                        IF(E.LT.LL) GO TO 320
                        GO TO 270
90                320   M = M + 1
                      R(1)=D(1)
                        IF(M.GE.2) GO TO 330
                      R(2)=D(1)
                        GO TO 310
95                330   DF = ((R(1) - R(2))**2)**0.5
                      R(2)=D(1)
                      F=((DF/D(1))**2)**0.5
                        IF(F.LT.LL) GO TO 260
                        GO TO 310
100               260   WRITE (6,66) NE,NPE,LL
                        WRITE (6,77) C(1),D(1)
                        WRITE (6,44)
                        WRITE (6,55)    ((J,I,A(J),B(J),T(J,I),Z(J,I),ZZ(J,I),I=1,NPE),J=1
                      2,NE)
105                     WRITE (6,88) SCT(K)
                        STOP
                        END
```

5 EXPERIMENTS, 20 POINTS IN EACH EXPERIMENT, PRECISION IS .00010

COMPUTER OUTPUT

C = .324E-01 D = .315E-02

I	A(J)	B(J)	T(J,I)	Z(J,I)	ZZ(J,I)
1	.469E+01	.186E+01	3.0	.800	.800
2	.469E+01	.186E+01	6.0	.400	.400
3	.469E+01	.186E+01	9.0	.000	.000
4	.469E+01	.186E+01	10.0	.000	.000
5	.469E+01	.186E+01	12.0	.000	.000
6	.469E+01	.186E+01	15.0	.000	.000
7	.469E+01	.186E+01	30.0	.000	.000
8	.469E+01	.186E+01	45.0	.000	.000
9	.469E+01	.186E+01	60.0	.000	.000
10	.469E+01	.186E+01	75.0	.000	.000
11	.469E+01	.186E+01	90.0	.000	.000
12	.469E+01	.186E+01	105.0	.000	.000
13	.469E+01	.186E+01	120.0	.000	.000
14	.469E+01	.186E+01	135.0	.000	.000
15	.469E+01	.186E+01	150.0	.000	.000
16	.469E+01	.186E+01	165.0	.000	.000
17	.469E+01	.186E+01	180.0	.000	.000
18	.469E+01	.186E+01	195.0	.000	.000
19	.469E+01	.186E+01	210.0	.000	.000
20	.469E+01	.186E+01	225.0	.000	.000
1	.472E+01	.187E+01	3.0	.800	.800
2	.472E+01	.187E+01	6.0	.400	.400
3	.472E+01	.187E+01	9.0	.000	.000
4	.472E+01	.187E+01	10.0	.000	.000
5	.472E+01	.187E+01	12.0	.000	.000
6	.472E+01	.187E+01	15.0	.000	.000
7	.472E+01	.187E+01	30.0	.000	.000
8	.472E+01	.187E+01	45.0	.000	.000
9	.472E+01	.187E+01	60.0	.000	.000
10	.472E+01	.187E+01	75.0	.000	.000
11	.472E+01	.187E+01	90.0	.000	.000
12	.472E+01	.187E+01	105.0	.000	.000
13	.472E+01	.187E+01	120.0	.000	.000
14	.472E+01	.187E+01	135.0	.000	.000
15	.472E+01	.187E+01	150.0	.000	.000
16	.472E+01	.187E+01	165.0	.000	.000
17	.472E+01	.187E+01	180.0	.000	.000
18	.472E+01	.187E+01	195.0	.000	.000
19	.472E+01	.187E+01	210.0	.000	.000
20	.472E+01	.187E+01	225.0	.000	.000
1	.476E+01	.183E+01	3.0	.800	.800
2	.476E+01	.183E+01	6.0	.400	.400
3	.476E+01	.183E+01	9.0	.000	.000
4	.476E+01	.183E+01	10.0	.000	.000
5	.476E+01	.183E+01	12.0	.000	.000
6	.476E+01	.183E+01	15.0	.000	.000
7	.476E+01	.183E+01	30.0	.000	.000
8	.476E+01	.183E+01	45.0	.000	.000
9	.476E+01	.183E	60.0	.000	.000

10	.476E+01	.183E+01	75.0	4.900	4.904
11	.476E+01	.183E+01	90.0	5.200	5.220
12	.476E+01	.183E+01	105.0	5.450	5.471
13	.476E+01	.183E+01	120.0	5.800	5.806
14	.476E+01	.183E+01	135.0	5.900	5.856
15	.476E+01	.183E+01	150.0	6.000	5.993
16	.476E+01	.183E+01	165.0	6.100	6.105
17	.476E+01	.183E+01	180.0	6.200	6.190
18	.476E+01	.183E+01	195.0	6.300	6.276
19	.476E+01	.183E+01	210.0	6.300	6.351
20	.476E+01	.183E+01	225.0	6.300	6.379
1	.473E+01	.184E+01	3.0	.850	1.829
2	.473E+01	.184E+01	6.0	1.400	1.429
3	.473E+01	.184E+01	9.0	1.800	1.875
4	.473E+01	.184E+01	10.0	2.000	2.003
5	.473E+01	.184E+01	12.0	2.250	2.225
6	.473E+01	.184E+01	15.0	2.600	2.504
7	.473E+01	.184E+01	30.0	3.400	3.418
8	.473E+01	.184E+01	45.0	4.000	4.024
9	.473E+01	.184E+01	60.0	4.500	4.503
10	.473E+01	.184E+01	75.0	4.900	4.870
11	.473E+01	.184E+01	90.0	5.100	5.204
12	.473E+01	.184E+01	105.0	5.500	5.459
13	.473E+01	.184E+01	120.0	5.700	5.607
14	.473E+01	.184E+01	135.0	5.900	5.835
15	.473E+01	.184E+01	150.0	6.000	5.974
16	.473E+01	.184E+01	165.0	6.000	6.074
17	.473E+01	.184E+01	180.0	6.200	6.174
18	.473E+01	.184E+01	195.0	6.300	6.248
19	.473E+01	.184E+01	210.0	6.300	6.307
20	.473E+01	.184E+01	225.0	6.300	6.350
1	.464E+01	.191E+01	3.0	.900	1.852
2	.464E+01	.191E+01	6.0	1.400	1.462
3	.464E+01	.191E+01	9.0	1.900	1.918
4	.464E+01	.191E+01	10.0	2.100	2.044
5	.464E+01	.191E+01	12.0	2.300	2.268
6	.464E+01	.191E+01	15.0	2.600	2.548
7	.464E+01	.191E+01	30.0	3.500	3.455
8	.464E+01	.191E+01	45.0	3.900	4.055
9	.464E+01	.191E+01	60.0	4.500	4.518
10	.464E+01	.191E+01	75.0	4.900	4.908
11	.464E+01	.191E+01	90.0	5.200	5.206
12	.464E+01	.191E+01	105.0	5.400	5.456
13	.464E+01	.191E+01	120.0	5.600	5.662
14	.464E+01	.191E+01	135.0	5.900	5.827
15	.464E+01	.191E+01	150.0	6.000	5.961
16	.464E+01	.191E+01	165.0	6.100	6.071
17	.464E+01	.191E+01	180.0	6.200	6.159
18	.464E+01	.191E+01	195.0	6.250	6.231
19	.464E+01	.191E+01	210.0	6.300	6.290
20	.464E+01	.191E+01	225.0	6.300	6.338

SCT = .252E+00

```
      PROGRAM TSI (INPUT,OUTPUT,TAPE5=INPUT,TAPE6=OUTPUT)
      REAL SCT(5), DIFF(5), C(5), D(5), LL, R(2)
      REAL T(35,25),ZZ(35,25),X(35,25),Y(35,25),A(35),B(35)
      REAL Z(35,25),L(35)
   11 FORMAT(I4, I4, F8.5, F8.5, F8.5)
   22 FORMAT(F8.5)
   33 FORMAT(5(F6.1,F10.3))
   44 FORMAT(8X,*J*,16X,*I*,14X,*A(J)*,13X,*B(J)*,12X,*T(J,I)*,11X,*Z(J
     2,I)*,11X,*ZZ(J,I)*,///)
   55 FORMAT(07X,I2,15X,I2,11X,E10.3,7X,E10.3,9X,F6.1,9X,E10.3,7X,E10.3)
   66 FORMAT(*1*,17X,I2,5X,*EXPERIMENTS,*,5X,I2,5X,*POINTS IN EACH EXPER
     2IMENT,*,5X,*PRECISION IS *,F8.5)
   77 FORMAT(///,34X,*C = *,E10.3,25X,*D = *,E10.3,///)
   88 FORMAT(///,55X,*SCT = *,E10.3)
   99 FORMAT (*1*,10X,*D*,19X,*C*,18X,*DD*,18X,*DC*,18X,*SCT*,18X,*E*)
  111 FORMAT (5X,6(E10.3,10X))
      M = 0
      READ(5,11) NPE, NE, C(1), D(1), LL
      DO 21 J = 1,NE
      READ(5,22) L(J)
      READ(5,33) (T(J,I), Z(J,I), I=1,NPE)
   21 CONTINUE
      WRITE (6,99)
  310 DD = D(1)/1.9
      DC = C(1)/1.9
  270 K = 1
  110 SCT(K) = 0
      DO 31 J = 1,NE
      SY2 = 0
      SZX = 0
      SZY = 0
      SYX = 0
      SX2 = 0
      DO 41 I = 1, NPE
      X(J,I)=1.-EXP(-(L(J)*D(K)*T(J,I)))
      Y(J,I)=1.-EXP(-(L(J)*C(K)*T(J,I)))
      SY2 = SY2 + Y(J,I)**2
      SZX = SZX + Z(J,I)*X(J,I)
      SZY = SZY + Z(J,I)*Y(J,I)
      SYX = SYX + Y(J,I)*X(J,I)
   41 SX2 = SX2 + X(J,I)**2
      A(J) = (SY2 * SZX - SZY * SYX) / (SY2 * SX2 - SYX**2)
      B(J) = (SX2 * SZY - SZX * SYX) / (SY2 * SX2 - SYX**2)
      SC = 0
      DO 51 I = 1,NPE
      ZZ(J,I) = A(J) * X(J,I) + B(J) * Y(J,I)
   51 SC = (Z(J,I) - ZZ(J,I))**2 + SC
   31 SCT(K) = SCT(K) + SC
      DIFF(K) = SCT(1) - SCT(K)
   50 K = K + 1
      IF(K-3) 50, 60, 70
   50 D(2) = D(1) + DD
      C(2) = C(1)
      GO TO 110
   60 D(3) = D(1)
      C(3) = C(1) + DC
      GO TO 110
```

```
                  IF(K-5) 80, 90, 100
                  D(4) = D(1)
                  C(4) = C(1) - DC
                  GO TO 110
                  D(5) = D(1) - DD
                  C(5) = C(1)
                  GO TO 110
            100   IF(DIFF(2) - DIFF(3)) 120, 120, 130
            120   IF(DIFF(4) - DIFF(5)) 140, 140, 150
            140   IF(DIFF(5) - DIFF(3)) 160, 160, 170
            160   K = 3
                  GO TO 220
            170   K = 5
                  GO TO 220
            150   IF(DIFF(4) - DIFF(3)) 160, 160, 180
            180   K = 4
                  GO TO 220
            130   IF(DIFF(4) - DIFF(5)) 190, 190, 200
            190   IF(DIFF(5) - DIFF(2)) 210, 210, 170
            210   K = 2
                  GO TO 220
            200   IF(DIFF(4) - DIFF(3)) 210, 210, 180
            220   IF(DIFF(K)) 230, 230, 240
            230   DD = DD/2
                  DC = DC/2
                  GO TO 250
            240   D(1) = D(K)
                  C(1) = C(K)
            250   E=((DD/D(1))**2)**0.5
                  WRITE(6,11) D(K),C(K),DD,DC,SCT(K),E
                  IF(E.LT.LL) GO TO 320
                  GO TO 270
            320   M = M + 1
                  R(1)=D(1)
                  IF(M.GE.2) GO TO 330
                  R(2)=D(1)
                  GO TO 310
            330   DF = ((R(1) - R(2))**2)**0.5
                  R(2)=D(1)
                  F=((DF/D(1))**2)**0.5
                  IF(F.LT.LL) GO TO 260
                  GO TO 310
            260   WRITE (6,66) NE,NPE,LL
                  WRITE (6,77) C(1),D(1)
                  WRITE (6,44)
                  WRITE (6,55)    ((J,I,A(J),B(J),T(J,I),Z(J,I),ZZ(J,I),I=1,NPE),J=1
                 2,NE)
                  WRITE (6,88) SCT(K)
                  STOP
                  END
```

5 EXPERIMENTS, 20 POINTS IN EACH EXPERIMENT, PRECISION IS .00010

COMPUTER OUTPUT

C = .324E-01 D = .315E-02

I	A(J)	B(J)	T(J,I)	Z(J,I)	ZZ(J,I)
1	.469E+01	.186E+01	3.0	.800	.800
2	.469E+01	.186E+01	6.0	1.400	1.400
3	.469E+01	.186E+01	9.0	1.900	1.900
4	.469E+01	.186E+01	10.0	2.050	2.050
5	.469E+01	.186E+01	12.0	2.550	2.550
6	.469E+01	.186E+01	15.0	3.400	3.400
7	.469E+01	.186E+01	30.0	4.900	4.900
8	.469E+01	.186E+01	45.0	5.900	5.900
9	.469E+01	.186E+01	60.0	6.900	6.900
10	.469E+01	.186E+01	75.0	7.900	7.900
11	.469E+01	.186E+01	90.0	8.900	8.900
12	.469E+01	.186E+01	105.0	9.900	9.900
13	.469E+01	.186E+01	120.0	10.900	10.900
14	.469E+01	.186E+01	135.0	11.900	11.900
15	.469E+01	.186E+01	150.0	12.900	12.900
16	.469E+01	.186E+01	165.0	13.900	13.900
17	.469E+01	.186E+01	180.0	14.900	14.900
18	.469E+01	.186E+01	195.0	15.900	15.900
19	.469E+01	.186E+01	210.0	16.900	16.900
20	.469E+01	.186E+01	225.0	17.900	17.900
1	.472E+01	.187E+01	3.0	.770	.770
2	.472E+01	.187E+01	6.0	1.540	1.540
3	.472E+01	.187E+01	9.0	2.090	2.090
4	.472E+01	.187E+01	10.0	2.255	2.255
5	.472E+01	.187E+01	12.0	2.805	2.805
6	.472E+01	.187E+01	15.0	3.740	3.740
7	.472E+01	.187E+01	30.0	5.390	5.390
8	.472E+01	.187E+01	45.0	6.490	6.490
9	.472E+01	.187E+01	60.0	7.590	7.590
10	.472E+01	.187E+01	75.0	8.690	8.690
11	.472E+01	.187E+01	90.0	9.790	9.790
12	.472E+01	.187E+01	105.0	10.890	10.890
13	.472E+01	.187E+01	120.0	11.990	11.990
14	.472E+01	.187E+01	135.0	13.090	13.090
15	.472E+01	.187E+01	150.0	14.190	14.190
16	.472E+01	.187E+01	165.0	15.290	15.290
17	.472E+01	.187E+01	180.0	16.390	16.390
18	.472E+01	.187E+01	195.0	17.490	17.490
19	.472E+01	.187E+01	210.0	18.590	18.590
20	.472E+01	.187E+01	225.0	19.690	19.690
1	.476E+01	.183E+01	3.0	.735	.735
2	.476E+01	.183E+01	6.0	1.470	1.470
3	.476E+01	.183E+01	9.0	2.205	2.205
4	.476E+01	.183E+01	10.0	2.450	2.450
5	.476E+01	.183E+01	12.0	2.940	2.940
6	.476E+01	.183E+01	15.0	3.675	3.675
7	.476E+01	.183E+01	30.0	7.350	7.350
8	.476E+01	.183E+01	45.0	11.025	11.025
9	.476E+01	.183E+01	60.0	14.700	14.700

10	.476E+01	.183E+01	75.0	4.900	4.904
11	.476E+01	.183E+01	90.0	5.200	5.220
12	.476E+01	.183E+01	105.0	5.450	5.476
13	.476E+01	.183E+01	120.0	5.800	5.866
14	.476E+01	.183E+01	135.0	5.900	5.856
15	.476E+01	.183E+01	150.0	6.000	5.955
16	.476E+01	.183E+01	165.0	6.100	6.055
17	.476E+01	.183E+01	180.0	6.200	6.155
18	.476E+01	.183E+01	195.0	6.300	6.254
19	.476E+01	.183E+01	210.0	6.300	6.331
20	.476E+01	.183E+01	225.0	6.300	6.379
1	.473E+01	.184E+01	3.0	.850	.869
2	.473E+01	.184E+01	6.0	1.400	1.429
3	.473E+01	.184E+01	9.0	1.800	1.870
4	.473E+01	.184E+01	10.0	2.000	2.063
5	.473E+01	.184E+01	12.0	2.250	2.325
6	.473E+01	.184E+01	15.0	2.600	2.504
7	.473E+01	.184E+01	30.0	3.400	3.418
8	.473E+01	.184E+01	45.0	4.000	4.064
9	.473E+01	.184E+01	60.0	4.500	4.553
10	.473E+01	.184E+01	75.0	4.900	4.904
11	.473E+01	.184E+01	90.0	5.100	5.084
12	.473E+01	.184E+01	105.0	5.500	5.459
13	.473E+01	.184E+01	120.0	5.700	5.683
14	.473E+01	.184E+01	135.0	5.900	5.856
15	.473E+01	.184E+01	150.0	6.000	5.974
16	.473E+01	.184E+01	165.0	6.000	6.044
17	.473E+01	.184E+01	180.0	6.200	6.174
18	.473E+01	.184E+01	195.0	6.300	6.248
19	.473E+01	.184E+01	210.0	6.300	6.287
20	.473E+01	.184E+01	225.0	6.300	6.350
1	.464E+01	.191E+01	3.0	.900	.865
2	.464E+01	.191E+01	6.0	1.400	1.462
3	.464E+01	.191E+01	9.0	1.900	1.918
4	.464E+01	.191E+01	10.0	2.100	2.044
5	.464E+01	.191E+01	12.0	2.300	2.268
6	.464E+01	.191E+01	15.0	2.600	2.548
7	.464E+01	.191E+01	30.0	3.500	3.455
8	.464E+01	.191E+01	45.0	3.900	4.052
9	.464E+01	.191E+01	60.0	4.500	4.561
10	.464E+01	.191E+01	75.0	4.900	4.908
11	.464E+01	.191E+01	90.0	5.200	5.206
12	.464E+01	.191E+01	105.0	5.400	5.455
13	.464E+01	.191E+01	120.0	5.600	5.602
14	.464E+01	.191E+01	135.0	5.900	5.827
15	.464E+01	.191E+01	150.0	6.000	5.966
16	.464E+01	.191E+01	165.0	6.100	6.071
17	.464E+01	.191E+01	180.0	6.200	6.159
18	.464E+01	.191E+01	195.0	6.250	6.231
19	.464E+01	.191E+01	210.0	6.300	6.290
20	.464E+01	.191E+01	225.0	6.300	6.330

SCT = .252E+00